EXPRESSION OF A SLOW MUSCLE MYOSIN (β-MyHC) DRIVES BOTH PHYSIOLOGICAL & PATHOLOGICAL CHANGES IN SKELETAL MUSCLE

by

GENEVIEVE CHRISTELLE KERR WILSON

B.A., Colorado College, 2012

A thesis submitted to the

Faculty of the Graduate School of the

University of Colorado in partial fulfillment

of the requirement for the degree of

Doctor of Philosophy

Department of Molecular Cellular and Developmental Biology

2019

This thesis entitled:
Expression of a Slow Muscle Myosin (β-MyHC) Drives Both Physiological & Pathological Changes in Skeletal Muscle
written by Genevieve Christelle Kerr Wilson
has been approved for the
Department of Molecular, Cellular and Developmental Biology

_____

Dr. Kenneth Krauter (Committee Chair)

_____

Dr. Leslie A. Leinwand (Thesis Advisor)

Date _____

The final copy of this thesis has been examined by the signatories, and we find that both the content and the form meet acceptable presentation standards of scholarly work in the above mentioned discipline.

IACUC Protocol# 2351

Wilson, Genevieve Christelle Kerr (Ph.D., Molecular, Cellular and Developmental Biology)
Expression of a Slow Muscle Myosin (β-MyHC) Drives Both Physiological & Pathological Changes in Skeletal Muscle
Thesis directed by Leslie A. Leinwand

ABSTRACT

Skeletal muscle is the most abundant and adaptable tissue in the human body, composed of muscle fibers which have the ability to respond to a variety of physiological and pathological stimuli, acting on the body's needs. Muscle fibers are composed largely of myosin, a highly conserved protein which interacts with actin and other sarcomeric proteins to generate the force needed for muscle contraction. Myosins are highly specialized being specific for varying tissue types and are characterized as slow or fast dependent on their biological properties. To better characterize the role of β-myosin (a slow myosin motor), how it responds to and drives physiological and pathological changes in skeletal muscle, we generated and studied novel animal models.

Forced expression of β-myosin (β-MyHC) in fast-type skeletal muscle identified a physiological role for β-MyHC in fiber type specification and plasticity. We showed that β-MyHC transgenic muscle has significantly increased PGC-1α, exhibits a fast-to-slow fiber type shift, increased oxidative metabolism, increased mitochondrial biogenesis, and resistance to fatigue. By sending a signal downstream, β-MyHC activates physiological and metabolic changes within skeletal muscle. Additionally, we created the first mouse model for a progressive skeletal muscle disease, Laing distal myopathy (MPD1), by expressing the R1500P rod mutation. We observed phenotypes which closely mimic MDP1 in our transgenic animals including muscle-specific functional and structural effects. Furthermore, we observed how this mutation is able to impact contractility parameters which provide new insight into how a rod domain mutation may lead to

disease. Changes in myosin isoform expression, specifically β-myosin, are able to drive physiological and pathological responses in skeletal muscle in ways that were previously unidentified. These mouse models can be used in future studies to further elucidate new roles for β-MyHC and its effect/role in skeletal muscle and to act as platforms for testing future therapeutic interventions.

ACKNOWLEDGEMENTS

I would like to thank my advisor, Dr. Leslie Leinwand, for her unwavering support and for allowing me to join the lab as a first-year graduate student. Your passion for science, your encouragement in helping me pursue my research projects, and your love of all thing's food (which I share) helped me grow as a scientist and ensured a successful graduate school career. I would also like to thank my fellow graduate students, post-doctoral researchers and really just everyone in the Leinwand lab for their help and support over the past several years. I truly could not have asked for a better lab environment to grow as a graduate student – you made things educational & productive while simultaneously making them fun. I would especially like to thank Massimo and Chicca Buvoli – my fellow bay mates – as without them, the research projects I undertook would not have existed. They were there for every scientific discussion, for every question – and most importantly, they were there for me in all aspects of my personal life and I couldn't be more grateful. I would like to thank my thesis committee for all of their helpful discussion and advice over the years. I would also like to thank all of my collaborators who helped make these projects a success. Finally, I would like to thank my friends and family for all of their love and support over the years – you got me through all of the ups and downs that inevitably come with the high level of stress that graduate school entails and you got me through before having a mental break-down. To my parents, I would not be here and in this career if it weren't for both of you – you encouraged me to pursue my scientific interests and to never be discouraged by failure. To my sister, you are my fellow scientific nerd and smart cookie – your passion and drive for the things that you love have always encouraged me to give each and everything I do my all. To my husband, you say each and every day that you have no understanding of

what I do but you have always supported me and loved me none-the-less. And lastly, to my dog – Kiera - you made graduate school bearable and sat by my side, while groaning and huffing as you would prefer to be outside, through every step of this thesis.

DEDICATION

This thesis is dedicated to my family, whose unwavering confidence in me made this work a reality. Each and every one of you believed in me through every step of this process and without you by my side, none of this would have been possible.

TABLE OF CONTENTS

FIGURES

CHAPTER I

CHAPTER II

CHAPTER III

CHAPTER I

Introduction

~600 skeletal muscles within the human body allow us to perform voluntary movements, to breathe, and to have functional independence. Each muscle's individual function is determined in part by its fiber-type composition and its proportion of slow-to-fast type muscle fibers. While developmental processes determine each individual's genetically pre-determined ratio by regulating expression of skeletal myosin heavy chain isoforms, fiber type is plastic and has the ability to shift & change due to a variety of physiological and pathological processes. To better understand the role of myosin content in skeletal muscle, we studied i.) a physiological response to a change in myosin content in fast-type skeletal muscle and what happens when you shift the balance from fast-to-slow; and ii.) a pathological response to a mutation in a slow muscle myosin and how a missense mutation leads to a progressive skeletal muscle disease, Laing distal myopathy.

Skeletal Muscle Biology

Skeletal muscle is the most abundant and adaptable tissue in the mammalian body, making up approximately 40% of total body weight (1). Skeletal muscle contributes to several bodily functions including generating the force and power needed to produce movement, to engage in activity, to maintain posture, and to allow for functional independence. However, while skeletal muscle is vitally important for bodily mechanics, it is also important for metabolism, respiration, and acts as a reservoir of amino acids required by other tissues (2–4). When skeletal muscle function is disrupted or impaired, a reduction in muscle mass occurs which negatively impacts the body's ability to respond to stress and/or disease.

Skeletal muscle is made up of an arrangement of muscle fibers (also referred to as myofibers or muscle cells) and associated connective tissue. These muscle fibers are multinucleated, syncytial structures resulting from the fusion of multiple myogenic cells. Each muscle fiber is made up of thousands of myofibrils and contains an assembly of contractile units known as sarcomeres which are located within a continuous cytoplasm. The two most abundant proteins of the sarcomere are actin (thin filament) and myosin (thick filament). Myosin (further described below) acts as the pre-dominant molecular motor which binds to actin. The relationship between these two proteins, in conjunction with other sarcomeric proteins, allows for muscle contraction & relaxation.

Myosin & Myosin Isoforms

Myosin is a highly conserved protein found in all eukaryotic cells. It interacts with actin and other proteins of the sarcomere to generate the mechanical force needed for muscle contraction (5). Myosins constitute a diverse superfamily and have been divided into seven individual classes. Class II, or conventional, myosins are hexameric proteins consisting of 2 heavy chains (MyHC) and two pairs of non-identical light chains (5). Dimerization of the MyHCs results in a coiled-coil interaction that leads to the generation of a polar structure which has two functional domains: the head domain, or motor domain, containing the enzymatic activity of the molecule, and the rod domain that drives assembly of the myosin into thick filaments (6). The coiled-coil sequence of the MyHC rod is divided into a series of 28 amino acid repeating units and consists of 4 heptads (d e f g a b c) (Figure 1.1A). Charged residues primarily occupy positions e and

g, while apolar or hydrophobic amino acids are generally found in positions a and d as their interactions are responsible for coiled-coil folding and stability (7).

A

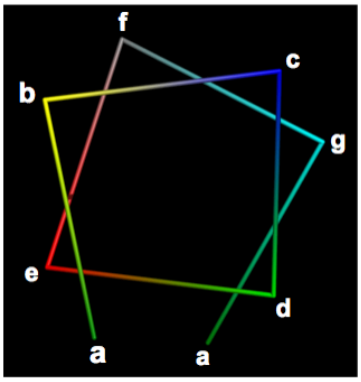

B

Gene	Protein	Muscle Fiber Type
MYH4	2B-MyHC	Fast 2B Fibers
MYH1	2X-MyHC	Fast 2X Fibers
MYH2	2A-MyHC	Fast 2A Fibers
MYH7	β-MyHC	Heart Slow Muscle Fibers
MYH6	α-MyHC	Heart
MYH3	Emb-MyHC	Developing Muscle
MYH8	Peri-MyHC	Developing Muscle

Figure 1.1. Myosin coiled-coil structure and striated myosin heavy chain isoforms.
(A) Structure of myosin as shown by the coiled-coil heptad repeat.
(B) Striated myosin heavy chain isoforms expressed in muscle.

There are eight class II, sarcomeric, striated myosin isoforms which can be further classified into 3 groups: cardiac, skeletal and developmental (Figure 1.1B). The cardiac isoforms are: α-MyHC (MYH6) and β-MyHC (MYH7), both of which are located on chromosome 14. While these 2 isoforms are 92.8% identical, they are functionally distinct, with β-MyHC being much slower with regards to steady-state measurements and ADP release (8). Additionally, β-MyHC is not only found in cardiac tissue but in slow skeletal muscle fibers and is characterized as the slowest skeletal isoform. The other skeletal isoforms are found on chromosome 17 and include IIa-MyHC (MYH2), IIx-MyHC

(MYH1), and IIb-MyHC (MYH4), listed respectively from slowest to fastest. Lastly, the developmental isoforms are Emb-MyHC (MYH3) and Peri-MyHC (MYH8). Developmental isoforms are expressed in the developing embryo and are down regulated after birth as isoform switching occurs and the expression of other isoforms takes over. These mammalian MYH genes are all highly conserved not only at the isoform level but also at the species level, having thought to have emerged from multiple gene duplication events from a common ancestral myosin molecule (9, 10).

Muscle Fiber Type Specification

Muscle fibers are classified into two major types, slow and fast, differing in their physiological and contractile properties. Each muscle fiber type has its own identity with regards to contractile rate, response to neural input, and metabolism (4, 11). Slow-type muscle fibers (Type I) predominantly contain the type 1 myosin heavy chain isoform β-myosin (β-MyHC), carry out oxidative metabolism, and have a high mitochondrial content (12–14). In contrast, fast-type muscle fibers (Type II) contain IIa, IIx, and IIb myosin heavy chain isoforms and have a high glycolytic capacity, being able to generate a much greater amount of anaerobic energy (12, 13) (Figure 1.2). These fiber-type specific properties are due to regulation by a variety of biochemical and physiological systems. Furthermore, whole muscles can be characterized as slow or fast dependent on the proportion of slow- to fast-type muscle fibers that they possess. For example, the soleus muscle is a characterized as a slow-type muscle, whereas the extensor digitorum longus is a fast-type muscle (Figure 1.2)

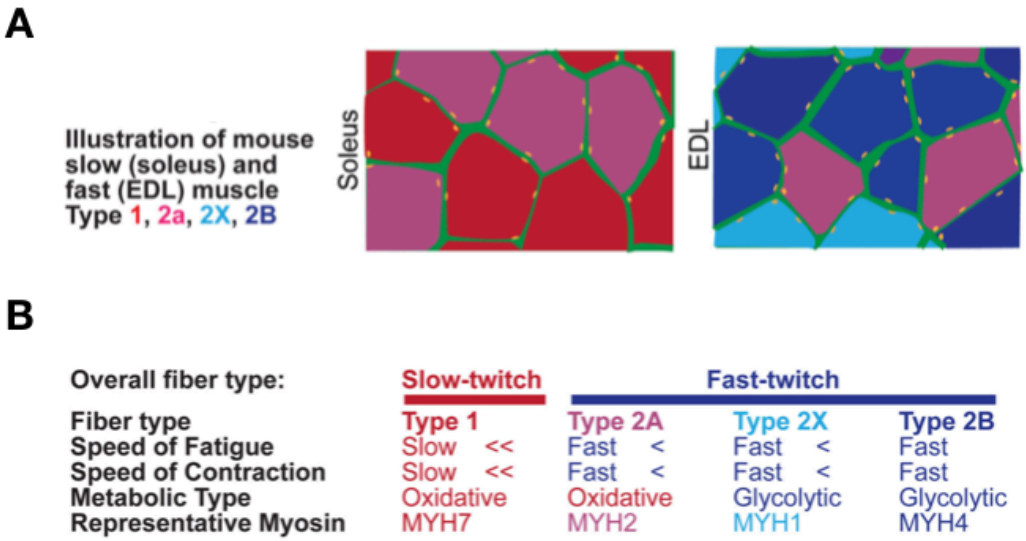

Figure 1.2. Skeletal muscle fiber types. Adapted from Talbot and Maves, 2016.
(A)Muscle groups, as illustrated in mouse, can be characterized as slow or fast dependent on the proportion of slow to fast muscle fibers they possess. Soleus is a characterized slow-type muscle made up of Type 1 and 2A fibers. EDL is a characterized fast-type muscle.
(B) Key properties of slow- and fast-type muscle fibers.

Once an embryo is generated, three germs layers – ectoderm, mesoderm, and endoderm – are formed. While each of these germ layers plays a unique role during development, the formation of most skeletal muscle begins from the mesoderm, which also gives rise to the heart, circulatory system, and kidneys. In response to developmental signals, the mesoderm forms somites which more largely develop into the dermomyotome, myotome, and sclerotome. Pax3 and Pax7, transcription factors expressed in the dermomyotome, act as myogenic progenitor cell-types (15, 16). Over time, to initiate the process of terminal differentiation, these cells express Myf5 or MyoD as committed myoblasts (17, 18). Skeletal muscle development continues through the

formation of committed myocytes with the expression of myogenin onto the formation of myotubes.

Myotube formation occurs over two stages giving rise to primary and secondary myotubes (19). Primary myotubes are formed from the fusion of early myoblasts, which eventually locate themselves between muscle tendons (19). Secondary myotubes are instead formed from the fusion of late-stage myoblasts, motor neurons provide the necessary signals for innervation. At this stage, both primary and secondary myotubes express their respective myosin heavy chains isoforms defining their muscle fiber-type (20–23). While genetic influences and motor neuron innervation developmentally account for differences in fiber type ratios amongst individuals, this ratio has the ability to change (discussed below).

More recently, mammalian, chicken, and zebrafish animal models have all shown how skeletal muscle fiber type is first determined during embryonic development through myogenic control mechanisms. Hedgehog signaling promotes slow-type fiber specification (24, 25), while the transcription factor SOX6 is generally expressed in fast-type muscle preventing the activation of slow-type genes (24, 26). Furthermore, homeodomain transcription factors within the SIX family, including SIX1 and SIX4, have also been shown to be required during embryonic development in order to promote a fast-type gene program (27, 28). SIX1 has been implicated in muscle plasticity (discussed below), since when expressed with its co-factor EYA1, the expression is sufficient to

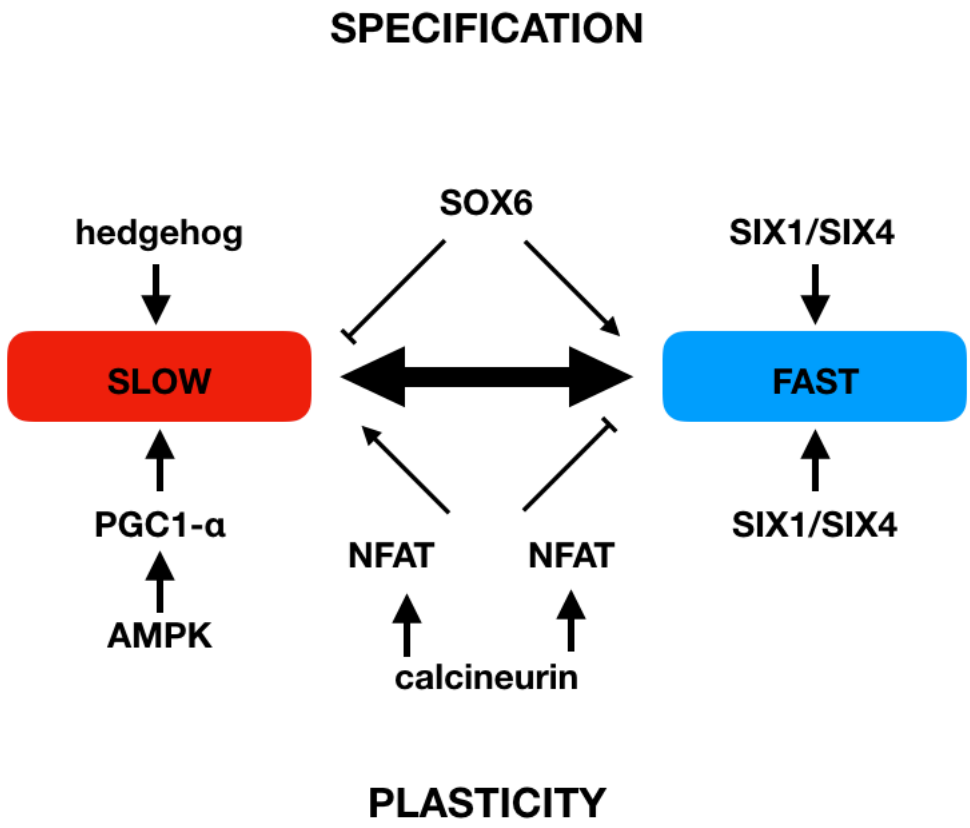

Figure 1.3. Signaling pathways that determine slow (red) or blue (fast) muscle fiber type. Specification pathways are shown on the top while plasticity pathways are shown on the bottom. Pathways are pre-dominantly separate; however, there is some overlap.

reprogram adult muscle fibers from slow to fast (29). While muscle specification and muscle plasticity are separate processes, they do utilize some of the same pathways.

However, while studies have implicated other signaling molecules in fiber-type determination, MYOD1 has been the most highly studied. MYOD1 is a member of the myogenic regulatory factor family and is necessary and sufficient for muscle specification and differentiation (30, 31). MYOD1 is involved in influencing both slow and fast fiber type specification by binding directly to DNA and regulating gene expression programs.

For example, SIX1 and SIX4 (mentioned above) directly bind several MYOD1 targets, including genes that control fast muscle differentiation(27, 32, 33).

Muscle Fiber Type Plasticity & Role in Disease

Skeletal muscles are plastic. During development and as a response to physiological or pathological stimuli, skeletal muscle fibers have the ability to undergo structural and metabolic remodeling, i.e., they are able to go through a fiber type transition. When there is a change in nerve signaling, hormones, or the levels of trophic factors, muscle fibers adapt and respond to these changes. However, while muscles are plastic, an individual's genetic make-up determines the extent to which muscle fibers can transition.

Pathways regulating fiber-type shift have been extensively studied, including the two major pathways calcineurin signaling and AMPK signaling. Calcineurin is a calcium-regulated serine/threonine phosphatase which acts as the primary mediator between neural input and its effect on muscle fiber-type (4, 34). Calcineurin activates NFAT transcription factors upon dephosphorylation. This in turn leads to the promotion of a slow-type phenotype while repressing a fast-type muscle phenotype (4, 11, 35). Recent studies have shown the role of NFATC1 in fiber-type switching in response to exercise, in addition to its benefits when studied in a mouse model for muscular dystrophy (36, 37). Similarly, AMPK signaling also promotes a slow, oxidative muscle phenotype. However, AMPK acts through PGC-1α, a transcription factor that functions in mitochondrial biogenesis (11, 36, 38, 39). In mice, PGC-1α is much more highly expressed in slow-twitch muscle fibers than in fast. Furthermore, when knocked out in mouse skeletal muscle, there is a shift towards faster muscle fibers including IIx and IIb (40).

Physiologically, the most common ways to induce a shift in muscle fiber-type are through a change in neural input and through exercise. Work first performed in 1960 by Buller et al. showed that in response to neural stimulation and changes in stimulation rate, muscle fibers are able to be reprogrammed from slow-to-fast or vice versa (41). In this original study, slow- and fast-twitch muscles were denervated and their proximal nerve segments were connected to a foreign nerve stump, otherwise known as cross-reinnervation. After cross-reinnervation, upon stimulation, it was observed that the isometric contraction time of the slow-twitch muscle had become much more like that of fast-twitch muscle and vice versa, simply by changing the neural input that the muscle received (41). Since this original study, work has been done to investigate the extent to which neural input affects muscle and how it exerts this control.

Similar to changes in neural input, exercise studies have shown that in response to different training programs, an individual is able to transition their muscle fibers from one type to the other. Classic studies have shown that untrained, average individuals have a 50/50 ratio of fast to slow-type muscle fibers. However, endurance athletes tend to average around 60% slow-twitch, whereas sprinters can have up to 80% fast-twitch. This shift in proportion of muscle fiber type also extends beyond running into other athletics such as weightlifting, as fiber type make-up is specialized to help perform different types of activities. While several studies have been performed examining changes in muscle fiber type in response to exercise, most have shown that training can shift type IIx fibers to IIa fibers and vice versa; the shift to Type I fibers has been less studied (42–44). However, studies have also shown that training and exercise can only allow for a modest shift in fiber-type going back to the idea of genetic pre-disposition.

Pathologically, there are many skeletal muscle diseases and other muscle-related disorders that have been shown to affect skeletal muscle fiber type including Duchenne

muscular dystrophy, myosinopathies, obesity/type 2 diabetes, and aging/sarcopenia. However, fiber type defects are not noted in all skeletal muscle diseases nor is it known why or how certain diseases preferentially affect one fiber-type over the other. Myosinopathies are diseases caused by mutations in the MYH genes, affecting both cardiac and skeletal muscle. Depending on the disease and in which MYH gene the mutation is found, both slow- and fast-type muscle fibers can be affected. Mutations in MYH7 affect Type I fibers, whereas mutations in MYH2 affect Type 2 fibers (45, 46). Obesity and type 2 diabetes have been shown to have more impact on Type I muscle fibers by significantly reducing their proportion in muscle, allowing for a greater number of Type II fibers (47). Age induced sarcopenia, or the loss of skeletal muscle mass and strength, is characterized in contrast by the loss of Type II muscle fibers, with Type I muscle fibers being unaffected (48). While these are only some examples, all of these studies help to relay the importance of understanding the effects on muscle fiber-type when it comes to disease and other health-related disorders.

Myopathies Caused by β-Myosin Mutations

More than 400 β-myosin mutations in the *MYH7* gene causing both cardiomyopathy and skeletal myopathy have been identified in human patients (http://www.hgmd.cf.ac.uk/ac/index.php) These myopathies are due to the expression of β-myosin in both cardiac muscle and slow skeletal muscle fibers. Mutations in the MYH7 gene are the common cause of hypertrophic cardiomyopathy (HCM), a condition that is characterized by thickening of cardiac muscle leading to an increased risk of heart failure; familial dilated cardiomyopathy (DCM), which leads to dilation of the left ventricular chamber and systolic dysfunction; and distal skeletal myopathies, which are

characterized by muscle atrophy and progressive muscle weakness. These disease-causing mutations are predominantly missense mutations in the globular head of myosin affecting the binding sites for actin; however, >100 mutations in the rod domain have been identified, with more being identified with continued scientific endeavors (http://www.hgmd.cf.ac.uk/ac/index.php). While β-myosin mutations leading to heart disease are a widely important area of study, this thesis will focus on *MYH7* gene mutations that to lead to skeletal myopathies.

While skeletal myopathies can be caused by mutations in each of the myosin heavy chain isoforms, mutations in β-myosin most commonly lead to myosin storage myopathy, Laing distal myopathy (discussed below), and scapuloperoneal and limb girdle syndromes. Myosin storage myopathy is widely known as a myosin aggregate myopathy due to accumulation of myosin (49). It is caused by mutations in the distal end of the tail of β-myosin, most commonly in exons 37-40 of MYH7. Symptoms tend to present from childhood into adulthood with initial weakness of the limb girdle, scapuloperoneal, or distal muscles. Clinical presentation is highly variable, ranging from patients being asymptomatic to having severe impairment and an inability to walk (49–52). Histological findings from muscle biopsies have shown protein aggregates present in Type I muscle fibers, myofibrillar disarray, and presence of filamentous structures. Although the more common manifestations of skeletal myopathies caused by MYH7 mutations are either myosin storage myopathy or Laing distal myopathy, there are cases that are unable to be classified into either group due to physical presentation. These patients are often classified as having limb girdle syndrome or scapuloperoneal myopathy presenting with weakness in these particular muscles without the morphological features of the other classified distal skeletal myopathies (53).

Laing Distal Myopathy

Laing distal myopathy (otherwise known as MPD1) is an autosomal dominant disease that affects skeletal muscle with the onset ranging from childhood to adulthood (53). It is initially characterized by weakness of the lower leg anterior compartment that affects ankle and great toe dorsiflexion, followed by disease progression to the proximal muscles (Figure 1.4A) (54). In spite of the high levels of β-myosin in the heart, cardiac involvement has been reported in only a few families (45, 53, 55–57). This it thought to be due to the presence of modifier genes, which could be preventing the development of a cardiac phenotype in humans, leading to the observed phenotypic variability. Although MPD1 progresses relatively slowly and is thought not to have an impact on life expectancy, it does have an impact on quality of life as many individuals become disabled or wheelchair confined. There are no uniform histologic hallmarks of MPD1 as histological findings are often variable (53). For example, it has been observed that there is a change in the overall size of Type I, or slow-twitch muscle fibers, with them being smaller than normal (Figure 1.4B). Additionally, there has been the indication of hybrid fibers or the co-expression of both slow and fast myosins within the same muscle fiber. Muscle biopsies have also shown mitochondrial abnormalities and the presence of minicores, in addition to mild necrosis and regeneration (53, 58).

MPD1-causing mutations have been mapped to the *MYH7* gene that encodes the β-myosin heavy chain, the primary myosin motor expressed in both human heart and in type I, slow skeletal muscle fibers (59). The majority of MPD1 mutations are located in the light meromyosin (LMM) domain corresponding to the C-terminal third of the rod that controls assembly of myosin into the thick filaments (56, 60, 61). However, a small number of them are also located in the motor domain (62, 63). The mutations in the rod

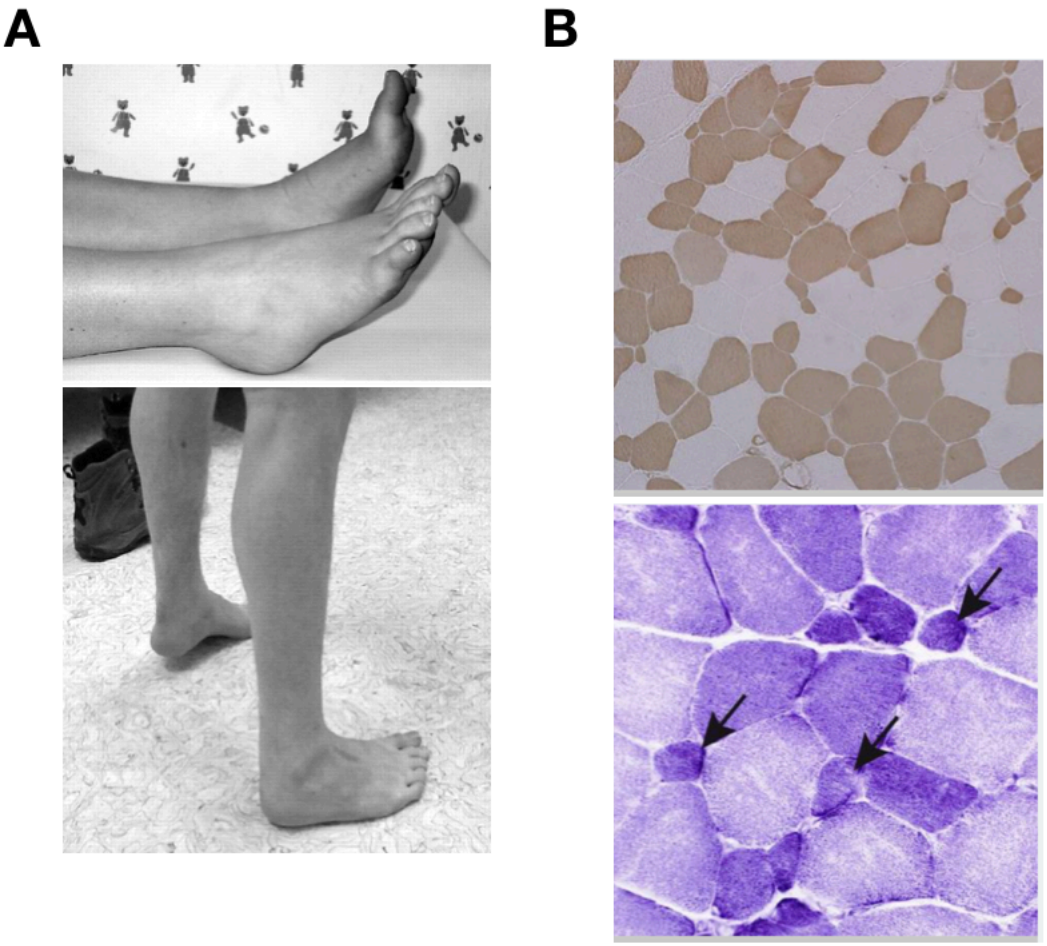

Figure 1.4. Laing distal myopathy clinical presentation and histological hallmarks.
(A) *Top*: 13-year-old attempting to dorsiflex both ankles but showing she is unable to. *Bottom*: 14-year-old demonstrating tightness of the Achilles tendon. Lamont et al., 2006.
(B) Muscle biopsies from a 7-year-old demonstrating hypotrophy of Type I muscle fibers. *Top*: ATPase Staining *Bottom*: NADH-TR staining. Tajsharghi and Oldfors, 2013.

primarily consist of codon deletions or missense mutations that result in the introduction of a proline residue (56, 60, 61). Amino acid deletions potentially affect folding and stability of coiled-coils by changing the configuration of apolar and charged residues along the heptad repeat, whereas the presence of proline residues in the coiled-coil is predicted to alter the structure of the coiled-coil by introducing a kink into the α-helix

axis (64). More recently, charge changing mutations involving glutamate to lysine amino acid changes have also been identified (56). Charge reversal mutations could affect the electrostatic interactions between adjacent myosin molecules.

Previous studies have begun characterization of several rod mutations associated with cardiomyopathy as well as distal myopathies, including looking at the effects of MPD1-causing mutation R1500P. Proline substitutions located within the coiled coil sequence of the MyHC rod were originally predicted to prevent incorporation of the thick filament into the sarcomere due to steric hinderance (60). To test this, biochemical characterization of this mutation was performed using a variety of assays which showed that the presence of a proline led to unique thermodynamic, structural, and functional differences. Specifically, the MPD1 amino acid substitution R1500P alters the thermodynamic stability and filament forming properties of light meromyosin *in vitro*. To further evaluate the effects of this particular mutation, studies were performed in cells and nematode-based systems continued to (65). Muscle cell-based studies have shown that proline rod mutations do not impair incorporation of the mutant myosins into the sarcomere (63) and therefore, do not block formation of the rod coiled-coil structure as originally proposed (60). However, they can trigger myosin cytoplasmic aggregates (63) or cause aberrant myosin packing in thick filaments (66). Studies performed in nematodes indicated that presence of the mutation did not affect muscle force generation or thick filament formation – even in the presence of myosin aggregates (67).

More recently, to characterize the molecular mechanisms of the MPD1-causing mutation L1729del, Dahl-Halvarsson et al. established a *Drosophila melanogaster* model for MPD1 (68). They showed that the deletion led to profound effects on muscle structure and function, including severely disrupting sarcomeric structure, reducing motility, and affecting lifespan, all phenotypes observed in patients with Laing distal myopathy.

Furthermore, they went on to show that overexpression of the *Drosophila* protein Abba/Thin was sufficient to alleviate some of the observed pathogenic phenotypes (68), suggesting that expression of this E3 ligase modifier gene may reduce or enhance the impact of this particular myosin mutation in humans. The effect of MPD1-causing mutations in a mammalian skeletal muscle have yet to have been observed, so it remains to be seen if these studies would mimic what was seen in the *Drosophila* model.

CHAPTER II

Expression of a Slow Myosin Motor (β-MyHC) Drives Physiology and Metabolism in Skeletal Muscle

Introduction

Skeletal muscle plays a large role in the human body as a regulator of voluntary movement. However, it is also critical for metabolism, energy storage, and energy consumption (4). Skeletal muscle is made up of specialized myofibers, or contractile units, which are grossly categorized into two major types – slow and fast – differing in their physiological, metabolic, and contractile properties (4, 69, 70). Slow-twitch (type I) muscle fibers express primarily the type I myosin heavy chain (MyHC) isoform which is also known as β-MyHC, carry out oxidative metabolism and have a high mitochondrial content (11, 13, 14). Fast-twitch (type II) muscle fibers express type IIa, IIx, and IIb MyHC isoforms, contain fewer mitochondria, rely on glycolytic metabolism for energy production, and are less fatigue resistant (11, 13). Each of these fiber types has a distinct metabolic profile due to their varying composition of myosin heavy chain isoforms and other metabolic genes (4).

Most muscles consist of a mixture of muscle fiber types; no muscle is purely one fiber type or the other. However, muscle fiber type has the ability to be altered in response to a variety of physiological and pathological stimuli (4, 11, 71). Endurance exercise training and caloric restriction shift the ratio towards slow-twitch muscle fibers to allow for increased resistance to fatigue and higher mitochondrial oxidative capacity (72–74). Conversely, skeletal muscle diseases such as Duchenne muscular dystrophy and myosinopathies in addition to age-induced sarcopenia reduce the number of slow-twitch muscle fibers due to skeletal muscle dysfunction and the need to burn energy more

quickly (45, 48, 75, 76). Regardless of directionality, this shift in the ratio of slow-to-fast muscle fibers is always accompanied by a shift in the composition of myosin heavy chains present in the muscle.

Several studies have previously identified pathways that regulate myofiber shifting with the idea that better understanding of the molecular mechanisms that regulate a switch from fast-to-slow myofibers could allow for the development of potential therapeutics for the many diseases in which fiber type is affected. However, while the myosin heavy chain genes are important for defining muscle fiber type identity, the composition of these genes is thought to be determined by fiber-type specific signaling cascades that occur developmentally, including the calcineurin-NFAT and PGC-1α pathways (37, 38, 40). These regulatory decisions are determined by transcription factor binding motifs located within the promoter region of each of the MyHC genes (77). It remains to be seen if MyHC expression plays a role in muscle fiber type specification.

To bridge this gap, we generated and analyzed transgenic mice that express β-MyHC at high levels in fast-type skeletal muscles to determine if a change in the myosin isoform content is sufficient to change the physiology and metabolism of skeletal muscle. β-MyHC transgenic muscle has significantly increased PGC-1α, exhibits a fast-to-slow fiber type shift, increased oxidative metabolism, increased mitochondrial biogenesis, and resistance to fatigue. This fiber shift requires PGC-1α in which slow-type fiber specification is coupled to mitochondrial function. Mechanistically, β-MyHC targets Fnip1, a negative regulator of AMP-activated protein kinase (AMPK), a known activator of PGC-1α. Future directions aim to determine what signal β-MyHC is sending that leads to slow-type fiber specification and increased mitochondrial content and function. We also aim to determine if β-MyHC is functioning through multiple pathways. Finally, we aim to determine if, by increasing the level of β-MyHC in a Duchenne muscular

dystrophy background, we are able to ameliorate the pathophysiology observed in these animals.

Results

Transgenic expression of β-MyHC in fast-type skeletal muscle drives fast-to-slow fiber type shift

To study the potential role of β-MyHC in skeletal muscle fiber specification, we generated fast-type skeletal muscle specific β-MyHC transgenic mice. The transgenic (TG) lines were created under the control of the well characterized muscle creatine kinase (MCK) promoter that restricts transgene expression to fast skeletal muscle fibers only. As previously reported (78), we tracked expression of the transgene by tagging the C-terminal end of the mouse rod domain, which is 99% identical to the human homolog, with a myc-tag epitope. We obtained 3 transgenic lines which each expressed similar transgenic levels (Figure 2.1A). As a control, we used wild-type (WT) littermates that did not express the transgene (Figure 2.1A). In agreement with MCK promoter specificity (79), we did not detect transgene expression in any muscles that normally express detectable amounts of Type I/ slow myosin such as soleus and heart (Figure 2.1B).

Comparison of TG muscle weight and muscle weight/tibia length ratio showed there was a significant reduction when compared to WT controls (Figure 2.1C). There was no observed change in body weight (Figure 2.1C). To measure the level of expression of the different myosin heavy chain isoforms expressed in muscle, we performed quantitative real-time PCR (qRT-PCR). In addition to WT tibialis anterior (TA), WT soleus was used since it is a well-characterized slow-type muscle with a lack of transgene

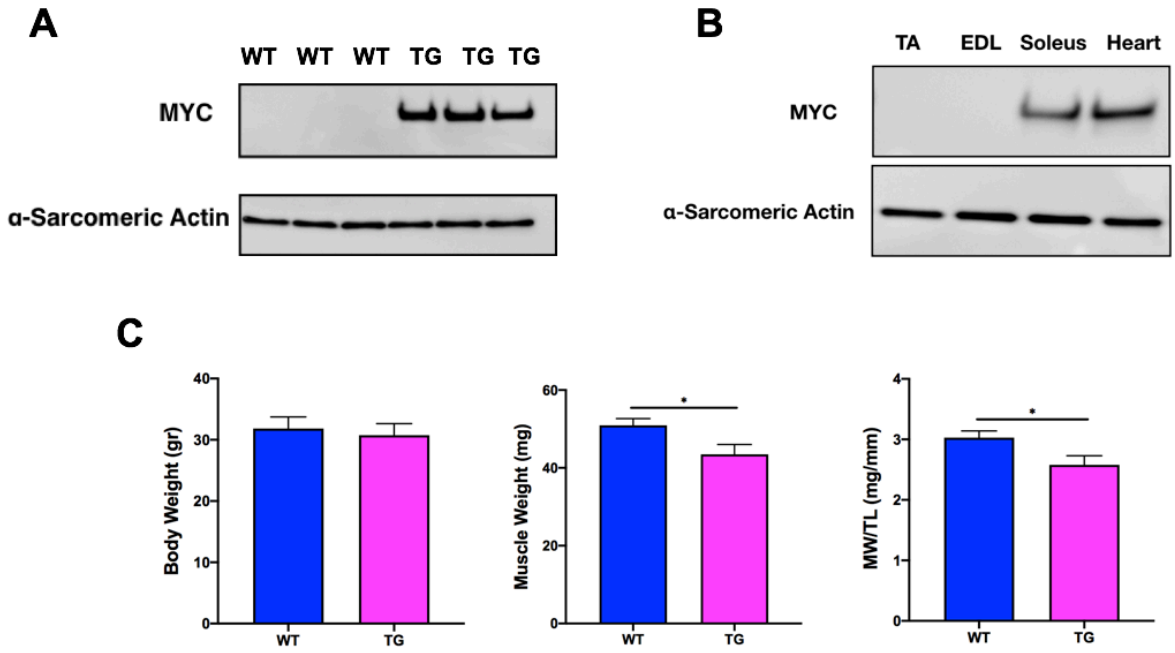

Figure 2.1. Generation of β-MyHC transgenic mice.

(A) Representative western blot analysis performed with tibialis anterior total protein extracts from the indicated genotypes using myc and α-sarcomeric actin (control) antibodies.

(B) Western blot analysis of transgene expression in different tissue types performed with total protein extracts from the indicated tissues using myc and α-sarcomeric actin (control) antibodies.

(C) Whole body weight, tibialis anterior muscle weight and muscle weight/tibia length ratio of WT and TG mice (n =20/group).

Data are expressed as mean +/- SEM. *$p < 0.05$ by two-tailed unpaired t-test with Welch's correction.

expression (Figure 2.1B). Furthermore, we wanted to determine in each of the performed assays whether TG muscle is more similar to characterized fast-type muscle (TA) or characterized slow-type muscle (soleus). We found that RNA from the slowest isoforms (Myh7 and Myh2) was significantly upregulated while there was a concomitant downregulation of RNA from the fastest isoform (Myh4) (Figure 2.2A). In addition, we measured the relative gene expression levels of markers of slow- and fast-twitch muscle

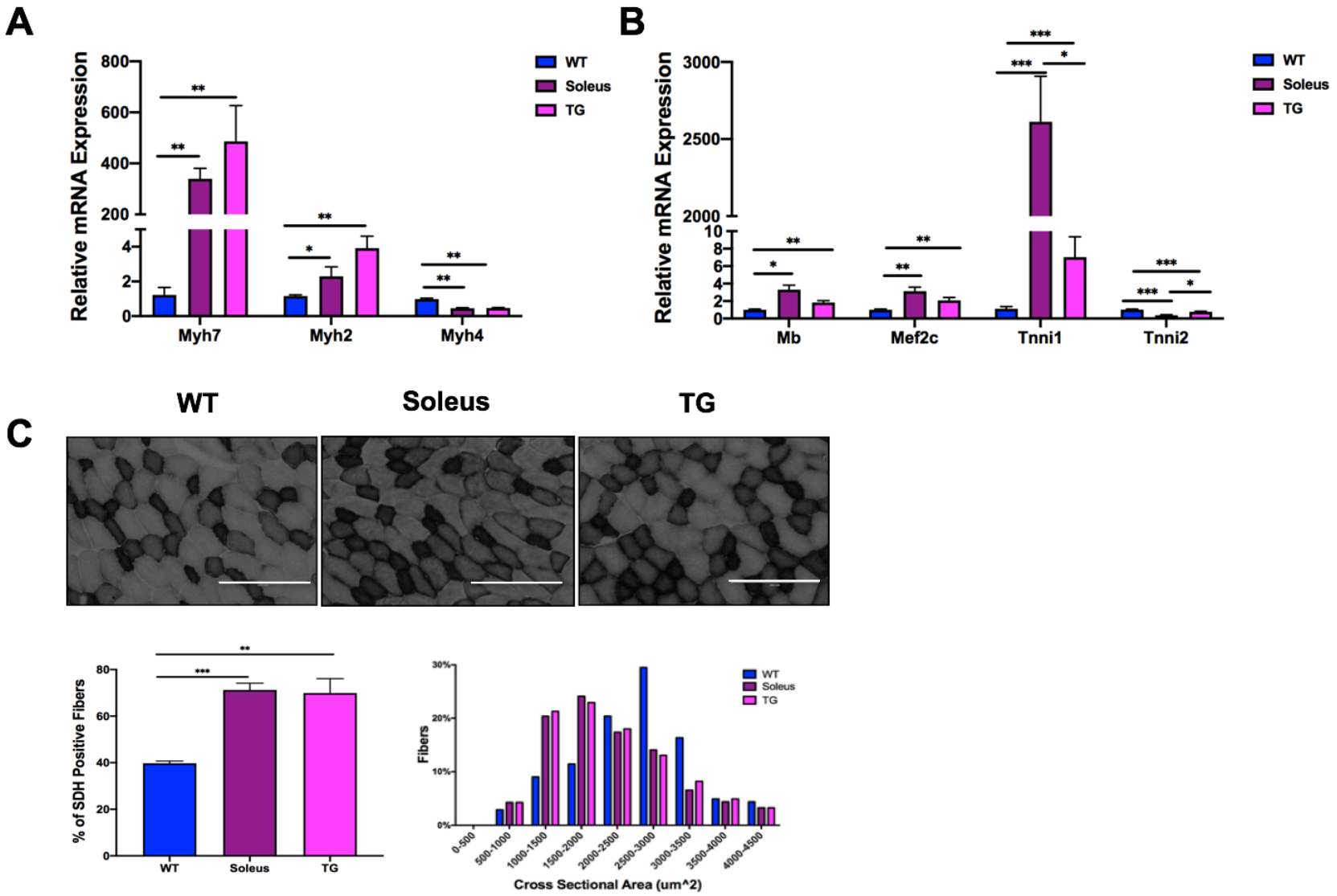
A
Relative mRNA Expression
800
600
400
200
4
2
0
Myh7
Myh2
Myh4
WT
Soleus
TG
B
Relative mRNA Expression
3000
2500
2000
10
8
6
4
2
0
Mb
Mef2c
Tnni1
Tnni2
WT
Soleus
TG
C
WT
Soleus
TG
% of SDH Positive Fibers
80
60
40
20
0
WT
Soleus
TG
Fibers
30%
20%
10%
0%
0-500
500-1000
1000-1500
1500-2000
2000-2500
2500-3000
3000-3500
3500-4000
4000-4500
Cross Sectional Area (um^2)
WT
Soleus
TG

Figure 2.2. Expression of β-MyHC in fast-type muscle drives fast-to-slow fiber type switch.

(A) Relative mRNA expression levels of myosin heavy chain isoforms in the tibialis anterior/soleus muscle from WT and TA muscle from TG mice (n = 10/group).
(B) Relative mRNA expression levels of Mb, Mef2c, Tnni1, and Tnni2 in the tibialis anterior/soleus muscles from WT mice and the TA from TG mice (n = 8/group).
(C) Representative SDH activity as shown by staining cross-sections of tibialis anterior/soleus muscles from WT mice and TA from TG mice. Quantification of percentage of SDH positive muscle fibers and muscle fiber size are also shown. Bar(s) corresponds to 200 um.

Data are expressed as mean +/- SEM. *p < 0.05, **p < 0.01, ***p < 0.001 by two-tailed unpaired t-test with Welch's correction.

fibers and found there was an increase in oxidative markers such as myoglobin (*Mb*), slow troponin (*Tnni1*), and myocyte enhancer factor 2C (*Mef2c*) while there was a decrease in glycolytic markers such as fast troponin (*Tnni2*) (Figure 2.2B). Histological analysis of WT TA and soleus and TG TA muscle enzymatically stained for the mitochondrial enzyme succinate dehydrogenase (SDH) showed a significant increase in the percentage of SDH positive fibers (Figure 2.2C), with similar levels being observed in the soleus. Furthermore, measurement of muscle fiber cross sectional areas showed a greater proportion of smaller muscle fibers, consistent with slow-twitch muscle fiber size (Figure 2.2C). Taken together, these data suggest that expressing β-MyHC in fast-type skeletal muscle results in a fiber type switch from fast-to-slow, with TG muscle more closely resembling characterized slow-type muscle.

Expression of β-MyHC increases oxidative mitochondrial function

To further define the slow-twitch phenotype observed in TG muscle, we next complemented these studies by analyzing TA muscle ultrastructure with transmission electron microscopy (TEM). Analysis indicated that mitochondria from TG mice were larger than those in WT controls (Figure 2.3A). This was complemented by quantification

of mitochondrial DNA content which showed a significant increase in the amount of mitochondrial cytochrome c oxidase subunit I (CO1). Similar levels were measured in the soleus (Figure 2.3B). Furthermore, measurement of relative gene expression levels of genes encoding a variety of mitochondrial-encoded genes (mt-*Nd2*, mt-*Co1*, and mt-*Co2*) and nuclear-encoded genes (*Cox7b* and *Atp5e*) that play a role in the electron transport chain were induced in TG TA muscle compared to WT controls (Figure 2.3C). We also found an increase in biomarker genes associated with fatty acid uptake and muscle glucose metabolism in TG muscle, including *Ldhb, Cd36*, and *Lpl* (Figure 2.3D). To functionally complement these studies, we measured respiration rates of isolated muscle fibers in response to pyruvate, a mitochondrial substrate that stimulates oxygen consumption. We found that pyruvate-driven mitochondrial respiration is higher in muscle fibers from extensor digitorum longus (EDL), a fast-type muscle, from TG animals when compared to WT (Figure 2.3E). EDL was used in this assay instead of TA due to the muscle fiber isolation protocol being followed. While this assay is only a sample size of 1 animal per genotype, together, these results demonstrate that expression of β-MyHC drives increased oxidative mitochondrial function in fast-type muscle.

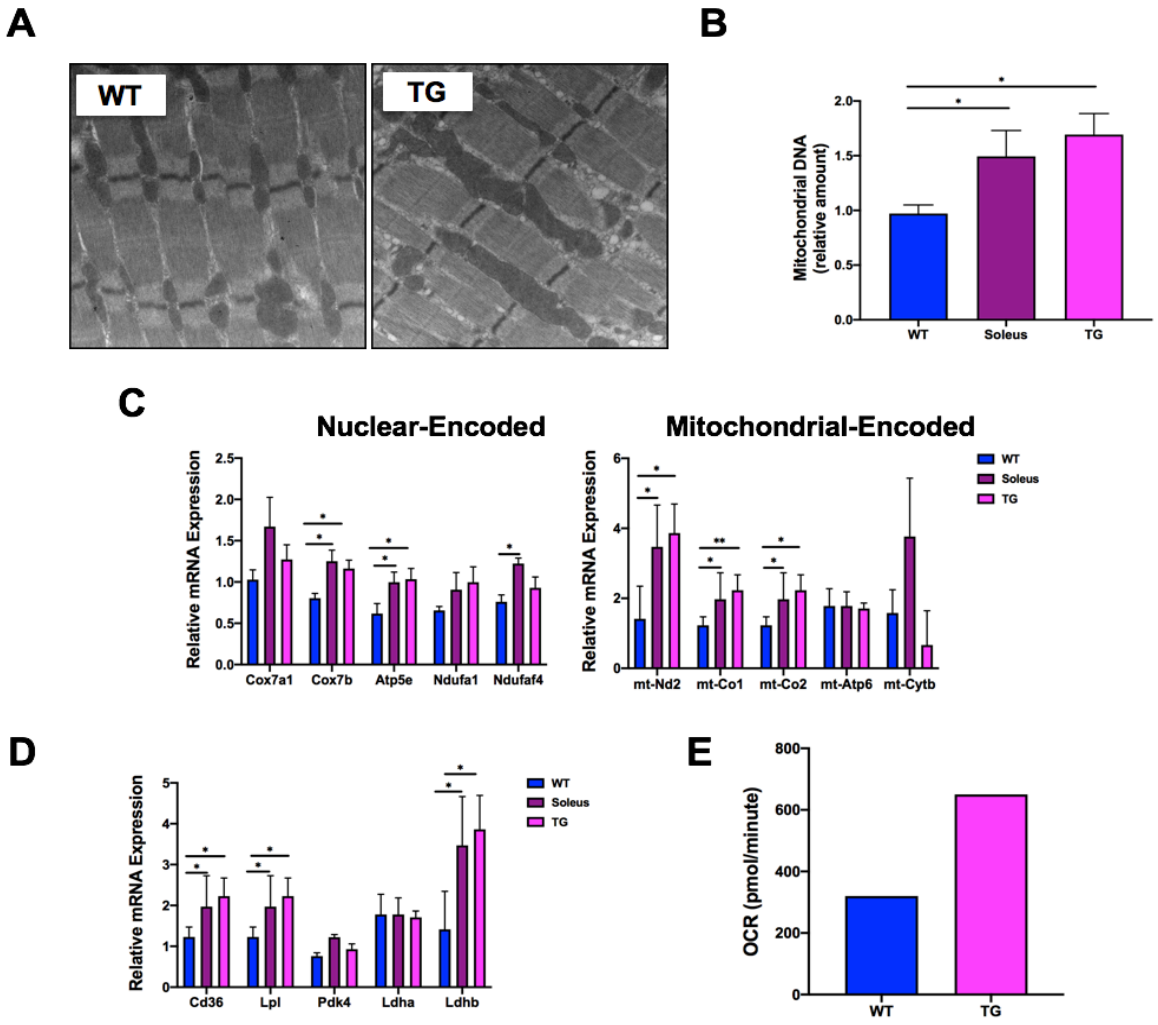

Figure 2.3. Expression of β-MyHC increases oxidative mitochondrial function.

(A) Representative electron microscopy images of TA muscle from WT and TG mice.

(B) Relative mitochondrial DNA content of CO1 normalized to 18S (n=6/group).

(C) Relative mRNA expression levels of nuclear- and mitochondrial-expressed electron transport chain (ETC) genes in TA and soleus muscle of WT and TG mice (n=6/group).

(D) Relative mRNA expression levels of genes involved in muscle glucose and fatty acid metabolism in TA and soleus muscle of WT and TG mice (n=6/group).

(E) Oxygen consumption rate measured in response to pyruvate of isolated myofibers from EDL muscle of TG mice and WT littermates. Myofibers within each genotype were pooled. (n=1/genotype)

Data are expressed as mean +/- SEM. *$p < 0.05$, **$p < 0.01$ by two-tailed unpaired t-test with Welch's correction.

β-MyHC expression increases exercise tolerance and fatigue resistance

Because a higher proportion of slow-twitch muscle fibers is commonly associated with increased endurance, we measured exercise tolerance and fitness in WT and TG mice using a fully automated tracking system to monitor voluntary wheel running. This analysis showed that total running distance over a 28-day period was significantly increased in 3-, 8- and 12-month-old male TG mice when compared to their WT counterparts (Figure 2.4A). Due to these results, we next evaluated *ex vivo* contractile function of the EDL muscle in WT and TG animals, since more sensitive parameters of muscle contraction and relaxation can be measured in an isolated muscle environment. EDL muscles were used instead of the TA due to the protocol requirement for intact muscle-tendon complexes (80). As a control, the properties of the slow-twitch soleus muscle were also analyzed. Measurements of tetanic and twitch force were performed after determining the optimal muscle length. Specific tetanic and twitch forces were observed to be significantly decreased in TG EDL (Figure 2.4B, 2.4C), an observation that is in agreement with results previously reported for muscles enriched with slow-type muscle fibers. Slow-type muscles tend to exhibit decreased force generation capacity (81). We next determined muscle fatigue by challenging the muscles with high frequency stimuli (100 Hz), which induced sustained muscle contraction; as the muscle relaxed over time, we measured the force output as an indicator of fatigue. The measurements obtained showed that the percentage of peak tetanic force dropped less quickly for TG muscle (Figure 2.4D). There were no observed differences when comparing soleus muscle

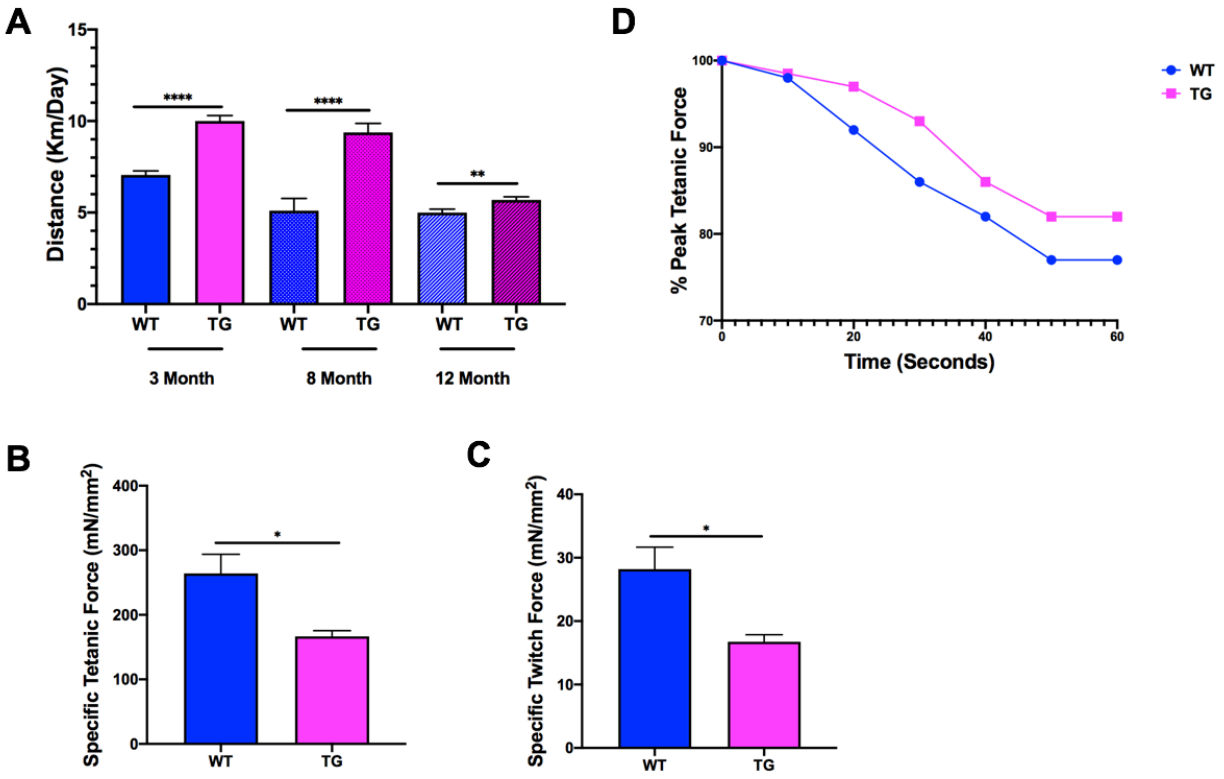

Figure 2.4. β-MyHC expression increases exercise tolerance and fatigue resistance.
(A) Male WT and TG mice were subjected to voluntary wheel running. Bars represent average running distance over 28 days (n = 10-12/group).
(B) Measurement of specific tetanic force in TG EDL compared to WT.
(C) Measurement of specific twitch force in TG EDL compared to WT.
(D) Percentage of force drop as EDL muscle relaxes after tetanic contraction, measured over 60 seconds (n = 1/group).
Data are expressed as mean +/- SEM. *$p < 0.05$, **$p < 0.01$ by two-tailed unpaired t-test with Welch's correction.

from either WT or TG animals. These data suggest that increased β-MyHC expression leads to production of muscle that has increased fatigue resistance accompanied by decreased force output allowing for increased endurance and greater exercise capacity.

Isolated β-MyHC TG muscle fibers display slow-twitch muscle fiber properties

To delve more deeply into the whole animal and whole muscle phenotypes of TG mice, we next analyzed force generation and relaxation kinetics of isolated myofibrils from TA muscle. Mounted myofibrils were activated and relaxed by rapidly switching between two flowing solutions of pCa 4.5 and pCa 9.0. After activation, rapid

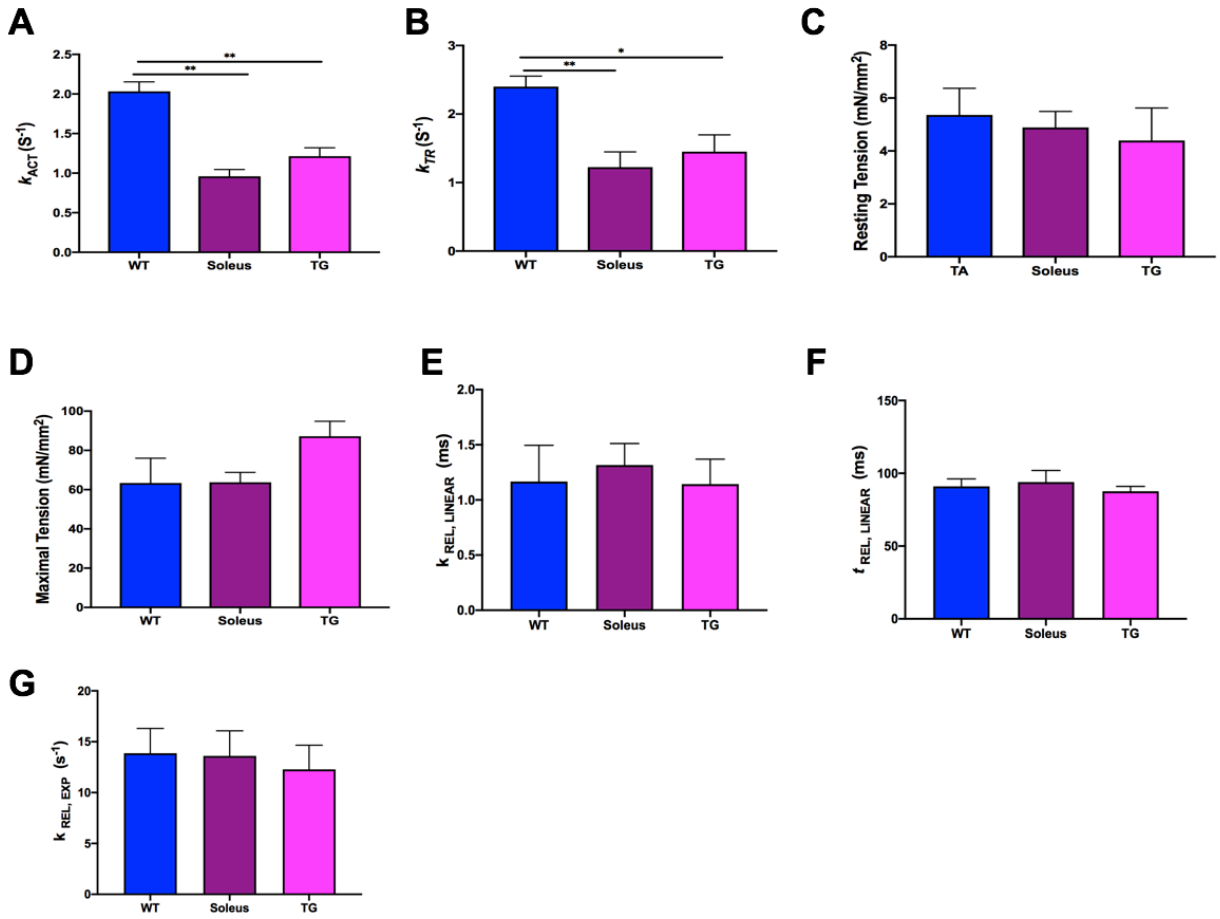

Figure 2.5. Isolated TG TA muscle fibers display slow-twitch contractile properties. Measured kinetics of activation and relaxation from myofibrils were as follows:

(A) The rate constant of tension development following maximal calcium activation.
(B) The rate constant of tension redevelopment following a release-restretch applied to the activated myofibril.
(C) Myofibril basal tension in fully relaxing condition.
(D) Maximal tension generated at full calcium activation (pCa 4.5).
(E) Rate constant of early slow force decline.
(F) Duration of early slow force decline.
(G) Rate constant of the final exponential phase of force decline.

Data are expressed as mean +/- SEM. *$p < 0.05$, **$p < 0.01$ by two-tailed unpaired t-test with Welch's correction.

deactivation of myofibrils follows a biphasic state: an initial slow linear decay precedes a faster exponential decay. Although we did not detect any changes in relaxation parameters, which include $k_{REL, LINEAR}$ (rate of slow phase relaxation), t_{REL} (duration of slow

phase relaxation), and $k_{REL,\ EXP}$ (rate of exponential relaxation) (Figure 2.5 E-G), we did observe that k_{ACT} and k_{TR} were significantly decreased when compared to WT (Figure 2.5A, 2.5B), with a similar decrease noted in the soleus. k_{ACT} is the rate constant of tension development following maximal calcium activation, whereas k_{TR} is the rate constant of tension redevelopment following a release-restretch applied to the activated myofibril. No changes were observed in resting or maximal tension (Figure 2.5 C, 2.5D). This decrease in myofibril activation kinetics has previously been observed when comparing slow-twitch to fast-twitch muscle fibers (82), reinforcing our previous results that suggest by changing the myosin isoform content, TG muscle more closely resembles slow-type muscle with regards to functional properties.

Increased activation of PGC-1α in β-MyHC TG muscle

We next sought to determine the potential targets and downstream pathways affected by increased β-MyHC expression to determine what other players are involved in the regulation of the slow-type phenotype observed. In order to do this, an RNA-Seq study was performed to compare differential gene expression between WT TA, WT soleus, and β-MyHC TA (further discussed in Chapter IV). PGC-1α is a key transcriptional regulator of mitochondrial biogenesis and function, previously identified in slow-twitch muscle fiber development. Measurement of gene expression levels of *Ppargc1a* (PGC-1α) and other factors associated with increased mitochondrial gene expression including *Ppargc1b* (PGC-1β) and *TFAM,* showed increased expression in RNA extracted from TG muscle (Figure 2.6A). Because of the observed upregulation of PGC-1α, we then went on to measure known upstream activators of PGC-1α, including Sirtuin 1 (SIRT1), a sensor and regulator of metabolism, and AMP activated protein kinase (AMPK), a master metabolic sensor which regulates slow-type muscle fiber development. Surprisingly, we found upregulation of SIRT1 mRNA and increased

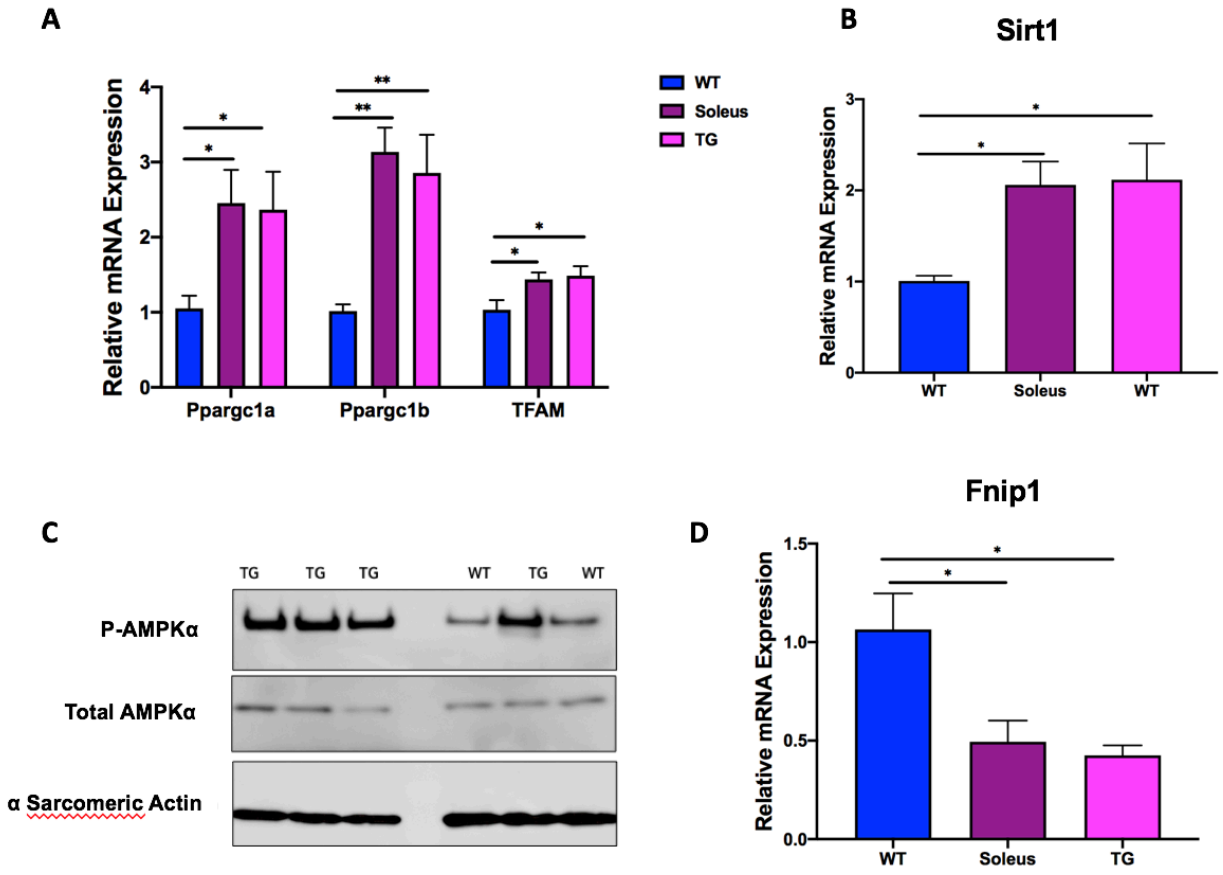

Figure 2.6. β-MyHC indirectly targets Fnip1 to activate AMPK-PGC-1α signaling.
(A) Relative mRNA expression levels of genes involved in slow-type muscle metabolism in TA and soleus muscle of WT and TG mice (n=6/group).
(B) Relative mRNA expression levels of SIRT1 (n = 6/group).
(C) Representative western blot analysis performed with tibialis anterior total protein extracts from the indicated genotypes using P-AMPKα, total AMPK, and α-sarcomeric actin (control) antibodies.
(D) Relative mRNA expression levels of Fnip1 (n = 6/group).
Data are expressed as mean +/- SEM. *p < 0.05, **p < 0.01 by two-tailed unpaired t-test with Welch's correction.

protein levels of phosphorylated AMPKα (total AMPKα was unaffected) (Figure 2.6B, 2.6C). These results indicate that multiple pathways may be activated by the change in expression of β-MyHC. However, we focused on the observed increase of phosphorylated AMPKα.

Reyes et al. published a novel role for folliculin interacting protein 1 (Fnip1), a known negative regulator of AMPK, that suggested a role for Fnip1 in the AMPK-PGC-1α regulatory pathway (81). Their findings showed that mice deficient in Fnip1 were more highly enriched for oxidative skeletal muscle. Because of these results, we measured gene expression of *Fnip1* in TG mice and observed a significant reduction when compared to WT TA, with similar levels being observed in WT soleus (Figure 2.6D). Together these results support a potential model in which β-MyHC indirectly targets Fnip1 to activate AMPK-PGC-1α signaling, allowing for the fast-to-slow fiber type shift observed in TG mice (Figure 2.9). Future/continued work aims to determine if this is the only pathway targeted by β-MyHC and/or if another pathway(s), potentially acting through SIRT1, is more highly or redundantly affected.

β-MyHC regulates fast-to-slow fiber type shift through PGC-1α

Because changes in β-MyHC expression led to increased levels of PGC-1α, we wanted to determine if the observed fast-to-slow fiber type shift was due to induction of PGC-1α. To do this, we bred β-MyHC TG mice with PGC-1α skeletal muscle specific knock-out (KO) mice to generate TG/PGC-1α mKO mice (Figure 2.7). Histological analysis of TA muscle from TG/PGC-1α mKO mice enzymatically stained for the mitochondrial enzyme succinate dehydrogenase (SDH) showed a significant decrease in the percentage of SDH positive fibers when compared to TG (Figure 2.8A). Additionally, measurement of the muscle fiber cross sectional area showed a greater proportion of larger muscle fibers (Figure 2.8A) in the TG/TG/PGC-1α mKO muscle sections. Furthermore, β-MyHC induction of oxidative biomarkers including myoglobin, *Ldhb*, and *Cox7b* was significantly reduced in the absence of PGC-1α (Figure 2.8B). Physiologically, with the disruption of PGC-1α, we also observed an effect with mice

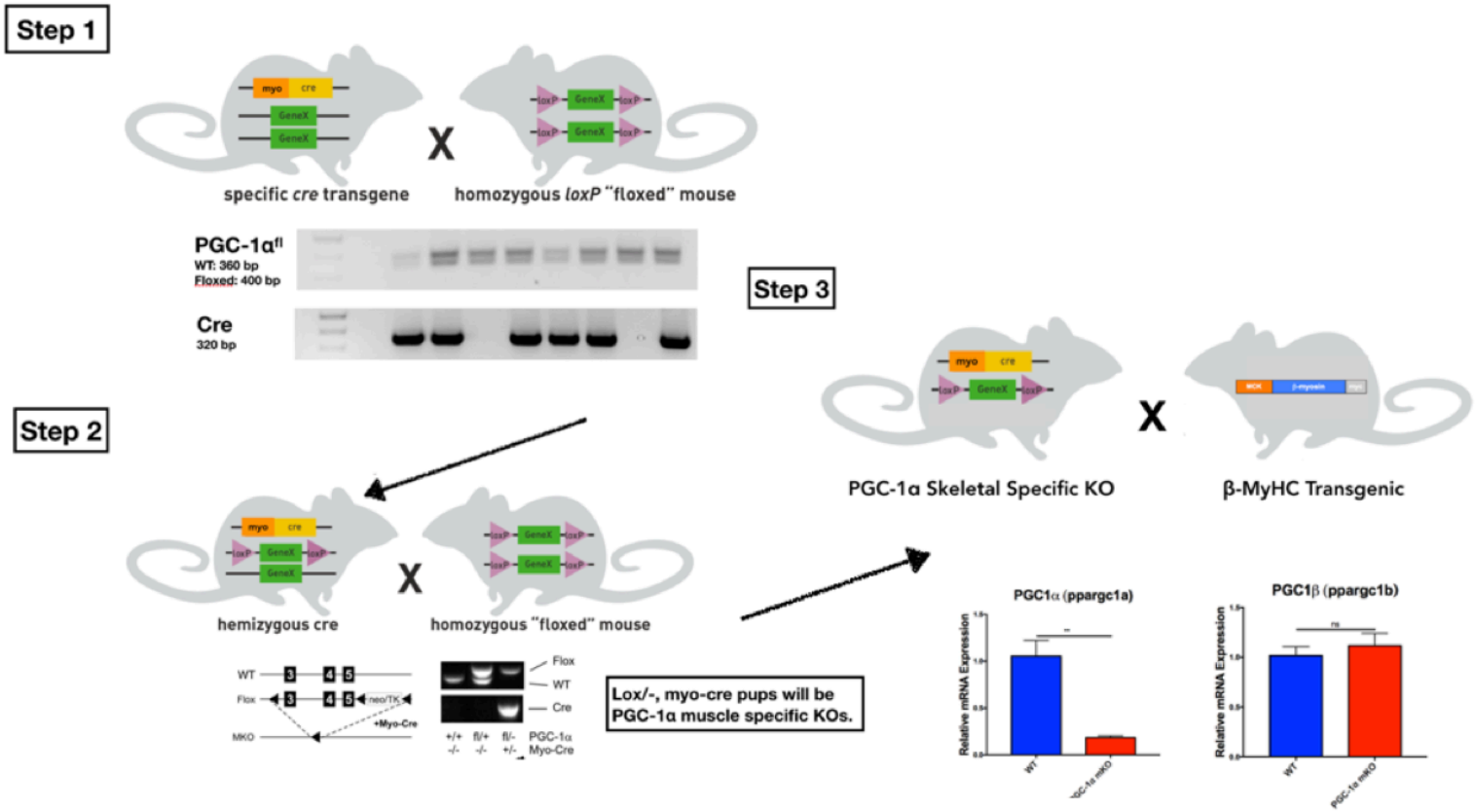

Figure 2.7. Generation of TG/PGC-1α mKO mice.

subjected to voluntary wheel running showing decreased exercise capacity. The average daily distance run was significantly decreased when compared to TG animals (Figure 2.8C). These results suggest that disruption of PGC-1α leads to reversion back to a fast-type phenotype and that PGC-1α is a key mediator of the oxidative fiber type shift observed in β-MyHC TG mice.

Discussion

Skeletal muscle is the most abundant and adaptable tissue in the mammalian body, composed of muscle fibers that are classified into two major types, slow and fast, differing in their physiological, metabolic and contractile properties. During development and as a response to physiological stimuli or disease, skeletal muscle fibers have the ability to undergo both structural and metabolic remodeling, shifting back and forth between fast and slow phenotypes. Due to the importance of this physiological phenomenon, pathways regulating this shift have been extensively studied. However, myosin heavy chain expression/determination has always been placed at the end of these

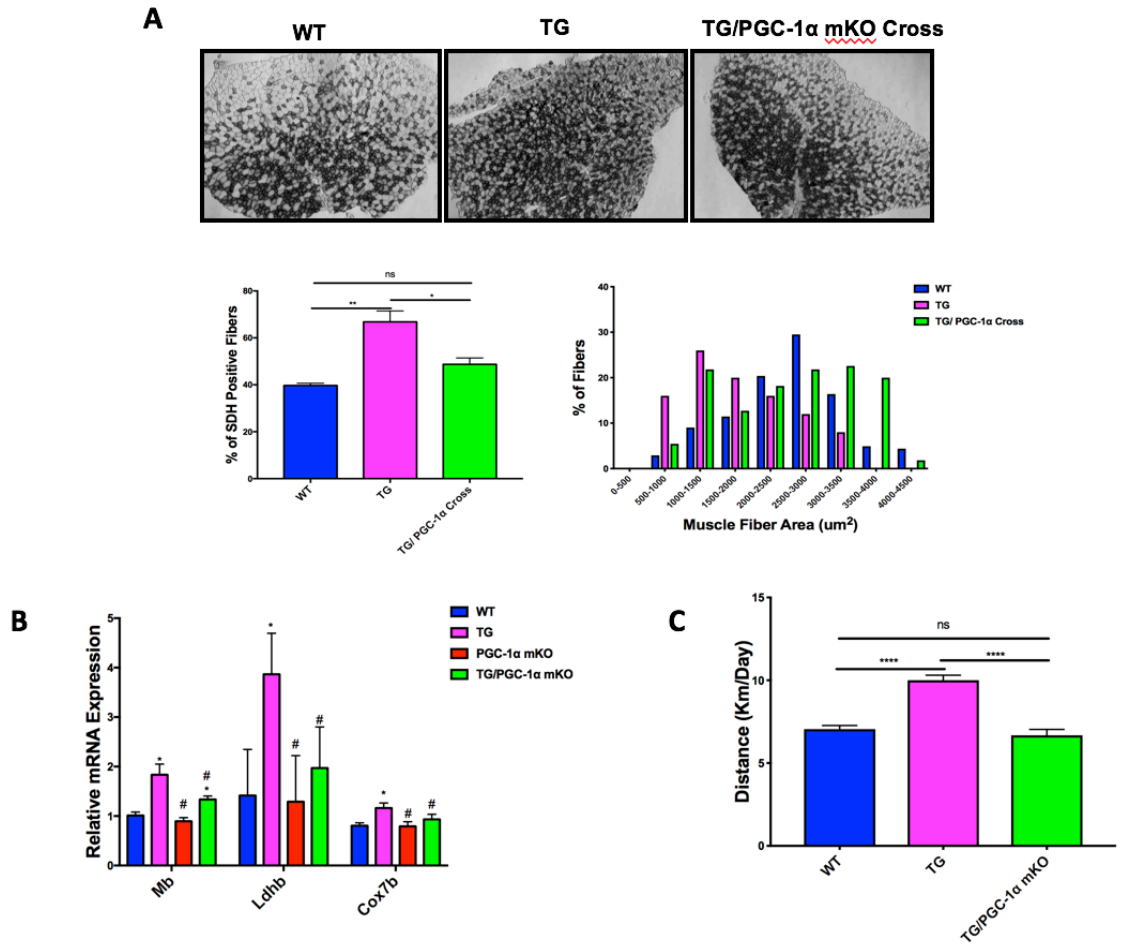

Figure 2.8. TG/PGC-1α mKO mice show reversion to fast-type phenotype.

(A) Representative SDH activity as shown by staining cross-sections of tibialis anterior muscle from WT, TG and TG/PGC-1α mKO mice. Quantification of percentage of SDH positive muscle fibers and muscle fiber size is also shown.

(B) Relative mRNA expression levels of oxidative biomarkers in the tibialis anterior muscle (n = 4/group; * versus WT , # versus TG).

(C) Male mice were subjected to voluntary wheel running. Bars represent average running distance over 28 days (n = 4/group).

Data are expressed as mean +/- SEM. *$p < 0.05$, **$p < 0.01$, ****$p < 0.001$ by two-tailed unpaired t-test with Welch's correction.

signaling cascades. Here, we generated a mouse model in which we forced expression of β-MyHC, a slow myosin motor, in fast-type skeletal muscle in order to identify a role for β-MyHC in fiber type specification and plasticity. Our studies provide evidence to support a potential model in which β-MyHC indirectly targets Fnip1 to activate AMPK-

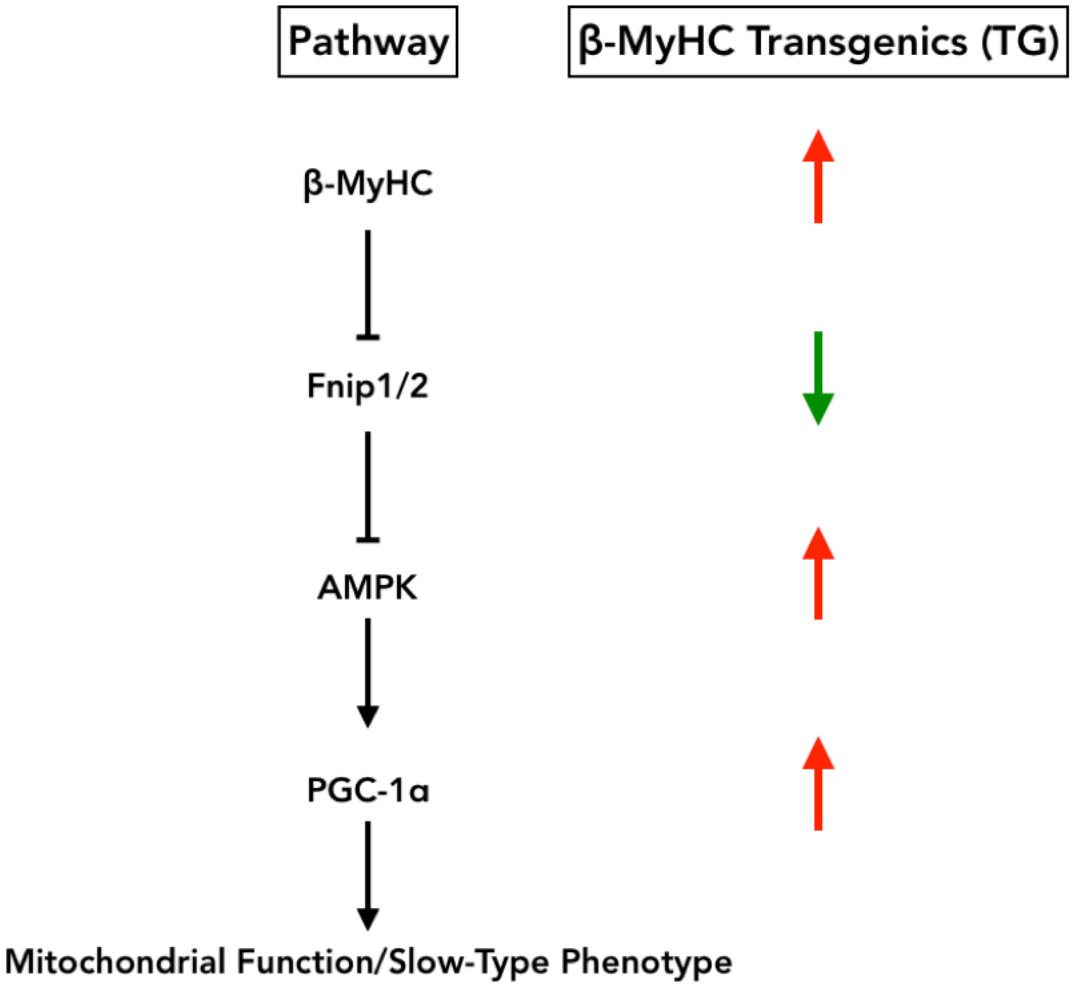

Figure 2.9. A potential pathway for β-MyHC regulation of fiber type and mitochondrial function in fast-type skeletal muscle.

PGC-1α signaling, allowing for the fast-to-slow fiber type shift and mitochondrial coupling observed in TG mice (Figure 2.9). This suggests, therefore, that myosin heavy chain isoforms may play a larger role in muscle fiber type specification than previously thought.

While we found that Fnip1 was significantly decreased in β-MyHC TG animals, suggesting a potential pathway for muscle fiber type specification, we also found that

SIRT1, a regulator of PGC-1α, was significantly increased to levels typically found in slow-twitch muscle. Muscle-specific SIRT1 gain-of-function has previously been shown to induce a fast-to-slow muscle fiber type shift, to increase levels of PGC-1α, to promote mitochondrial biogenesis, and to decrease expression of genes involved in muscle atrophy (83), similar phenotypes to those observed in β-MyHC TG animals. These results suggest that β-MyHC may be indirectly activating/targeting more than one pathway and that further studies are required in order to determine if this is the case.

As previously reported, β-MyHC is a structural protein whose primary function is to bind actin to regulate muscle contraction and relaxation (5). Because of this, regulatory decisions were thought to be determined by transcription factor binding motifs located within the promoter region of each of the MyHC genes (77), and not necessarily through expression of the myosin heavy chain isoform itself. While we have shown a potential pathway through which β-MyHC may be regulating muscle fiber type, we believe that β-MyHC is indirectly targeting members of the downstream pathway and that some sort of signal is being sent to trigger these signaling cascades. In 2000, a novel family of sarcomeric calcineurin binding proteins was identified known as the calsarcins. Calsarcin-1 is found in cardiac and slow-twitch skeletal muscle, whereas calsarcin-2 is restricted to fast skeletal muscle (84). Their discovery linked calcineurin with the contractile apparatus of the sarcomere as this family of proteins are proteins of the sarcomeric z-disc. While we did not measure expression of this family of proteins, it is possible that changes in transcription factors present at the z-disc are being regulated in a way in which the myosin isoform is present within the sarcomere. This opens up the question of whether the sarcomere recognizes changes in myosin isoform expression and if some sort of mechanical signal is being sent that activates subsequent downstream effects.

While our study showed that by changing β-MyHC expression in fast-type muscle, physiology and metabolism were regulated to become more like slow-twitch muscle, we did not see a complete conversion. Most of the performed assays demonstrated that β-MyHC TA was more like WT soleus than WT TA. However, while contractile genes were significantly downregulated in comparison to WT TA, they did not reach the much lower levels observed in WT soleus. The RNA-Seq analysis performed found that several genes including slow-type troponins and tropomyosin, all of which play a role in muscle contraction, were significantly different between β-MyHC TA and WT soleus. As these genes are regulated by calcium (Ca^{2+}) levels present in the cell, this could suggest that there are differences in Ca^{2+}-dependent gene expression programs or levels of Ca^{2+} activation between these two muscle groups and that β-MyHC is only able to regulate certain aspects of the slow-type gene program.

In summary, we generated a novel mouse model which suggested a new role for β-MyHC in muscle fiber type determination and specification. Continued efforts will be aimed at determining how β-MyHC is indirectly targeting these pathways and if changes in expression levels of β-MyHC are able to ameliorate pathophysiology of diseases in which a fiber type shift occurs.

Materials & Methods

Animal Care

All animal experiments were performed using protocols approved by University of Colorado Institutional Animal Care and Use Committees (IACUC). Animals were housed under standard conditions in a partial barrier facility and received access to water and

chow *ad libitum*. For sample collection, animals were sedated using 1-4% inhaled isoflurane and sacrificed by cervical dislocation. All data shown is from male mice.

Western Blotting

Protein lysates were prepared by homogenizing hindlimb muscle tissue in myosin extraction buffer (0.3M NaCl, 0.1M NaH2PO4, 0.05M Na2HPO4, 0.001M MgCl2.6H2O, 0.01M EDTA) following standard procedures. The antibodies used were against Myc-Tag (9B11) (1:10000, Cell Signaling Technology, #2276) and α-sarcomeric actin (1:2000). Protein lysates for other assays were prepared following standard procedures. The antibodies used were against AMPKα (Cell Signaling, #2603), and phospho-AMPKα (Cell Signaling, #2531). All blots were imaged using the ImageQuant LAS 4000 (GE Healthcare Bio-Sciences, Pittsburg, PA) system and analyzed with the ImageQuant software.

RNA Isolation & Quantification

Total RNA was purified from hindlimb muscles using TRI Reagent (Ambion) according to manufacturer's protocol. cDNA was synthesized using SuperScript III reverse transcriptase (Invitrogen) and random hexamer primers. Gene expression was determined by qRT-PCR using SYBR Green dye (Invitrogen) and gene specific primer sets. All genes were normalized to 18S expression. Data were collected and analyzed using Bio-Rad CFX Real-Time PCR system.

Histology (Succinate Dehydrogenase Staining)

Tibialis anterior muscles were snap frozen in isopentane/liquid N2, cryo-sectioned, and stained for enzymatic activities using standard procedures. The stained fibers were

counted and the percentage of total number of fibers was calculated (150–200 total fibers/image, 3 images/mouse, 2 mice/genotype). Cross sectional area was determined using ImageJ.

Transmission Electron Microscopy

Skeletal muscle was dissected and immersed in 2.5% glutaraldehyde and 2% paraformaldehyde in 0.1 M cacodylate buffer at pH 7.4 for a minimum of 24 hours at 4oC. For processing, the tissue was rinsed in 100 mM cacodylate buffer and then immersed in 1% osmium and 1.5% potassium ferrocyanide for 15 min. Next, the tissue was rinsed five times in cacodylate buffer, immersed in 1% osmium for 1 hour, and then rinsed again five times for 2 min each in cacodylate buffer and two times briefly in water. The tissue was stained en bloc with 2% uranyl acetate for 1 hour before it was transferred to graded ethanols (50, 70, 90, and 100%) for 15 minutes each. Finally, the tissue was transferred through propylene oxide at room temperature and then embedded in LX112 and cured for 48 h at 60oC in an oven. Ultra-thin sections (55 nm) were cut on a Reichert Ultracut S from a small trapezoid positioned over the tissue and were picked up on Formvar-coated slot grids or copper mesh grids (EMS). Sections were imaged on a FEI Tecnai G2 transmission electron microscope (Hillsboro, OR) with an AMT digital camera (Woburn, MA).

Seahorse Metabolic Analyses

EDL muscles were collected from WT and TG mice that were age- and sex-matched. Fresh tissue was rinsed in PBS and placed in a dissociation media composed of Dulbecco's modified Eagle medium (DMEM), gentamycin, 2% (vol/vol) FBS, and Collagenase A and left to incubate at 37 °C at 5% carbon dioxide for 1.5–2 h. Muscle samples were then

removed from dissociation media and gently triturated in DMEM until single muscle fibers were detached and suspended in solution. Isolated fibers of each genotype were combined and plated. After visualization under a dissecting microscope, fibers were counted and plated equivalently to achieve 80–90% confluence. Fibers were cultured in media in XF24 microplate (Seahorse Biosciences) and incubated at 37 °C for 6–12 h before analysis.

Functional Phenotypic Measurements

Voluntary Wheel Running

Male mice were subjected to voluntary wheel running for a period of 28 days at the age of 3 months, 8 months, and 12 months. Mice were housed individually in a large cage with a running wheel. Exercise time, velocity, and distance were recorded daily for each animal.

Ex-Vivo Contractility Assay

Mice were euthanized according to NIH guidelines and IACUC institutional animal protocols. Extensor digitorum longus (EDL) was carefully dissected in total from the ligamentary attachment at the lateral condyle of the tibia to the insertion region. The muscle was transferred to a dish containing ice-cold isotonic physiologic salt solution (Tyrode's buffer (mM): NaCl 118, KCl 4, MgSO4 1.2, NaHCO3 25, NaH2PO4 1.2, glucose 10 and CaCl2 2.5) bubbled with 95% O2/5% CO2 to maintain a pH of 7.4. The soleus was identified after removing the gastrocnemius muscle and was removed by cutting the ligaments connecting to the proximal half of the posterior tibia to the insertion, where the calcaneal tendon was cut, and the muscle was placed into ice-cold Tyrode's buffer. Muscles were mounted vertically in individual tissue bath chambers and maintained at

37° C. Muscles were stretched and optimal length was set for each muscle. Stimulatory trains of varying frequency (1-100 Hz) were used to generate force-frequency curves. Tetanic force was achieved in all muscles using 100 Hz.

Myofibril Isolation

Myofibrils were isolated from flash frozen soleus and tibialis anterior as described (85, 86). A small section of muscle was cut into thin slices and bathed in 0.05% Triton X-100 in Linke's solution (132mM NaCl, 5mM KCl, 1mM MgCl2, 10mM Tris, 5mM EGTA, 1mM NaN3, pH 7.1) with protease inhibitor cocktail (10 μM leupeptin, 5 μM pepstatin, 200 μM phenyl-methylsuphonylfluoride, 10 μM E64, 500 μM NaN3, 2 mM dithioerythritol) overnight at 4°C overnight. Skinned tissue was washed three times in rigor solution (50mM Tris, 100mM KCl, 2mM MgCl2, 1mM EGTA, pH 7.0) and resuspended in bath solution with protease inhibitors (pCa 9.0; 100mM Na2EGTA; 1M potassium propionate; 100mM Na2SO4; 1M MOPS; 1M MgCl2; 6.7mM ATP; and 1mM creatine phosphate; pH 7.0) and homogenized at medium speed for 10 seconds three times.

Myofibril Mechanics

Myofibrils were isolated and mechanical parameters were measured as described (86–88). Myofibrils were placed on a glass coverslip in relaxing solution at 15°C and then a small bundle of myofibrils was mounted on two microtools. One microtool was attached to a motor that produces rapid length changes (Mad City Labs) and the second microtool was a calibrated cantilevered force probe (5.8 μm/μN; frequency response 2-5 KHz). Myofibril length was set at 5-10% above slack length and average sarcomere length and myofibril diameter were measured using ImageJ. Mounted myofibrils were activated and relaxed by rapidly translating the interface between two flowing streams of solutions of

pCa 4.5 and pCa 9.0 (88, 89). Data was collected and analyzed using customized LabView software. Measured mechanical and kinetic parameters were defined as follows: resting tension (mN/mm2) – myofibril basal tension in fully relaxing condition; maximal tension (mN/mm2) – maximal tension generated at full calcium activation (pCa 4.5); the rate constant of tension development following maximal calcium activation (kACT); the rate constant of tension redevelopment following a release-restretch applied to the activated myofibril (kTR) (90); rate constant of early slow force decline (kREL, LIN) - the slope of the linear regression normalized to the amplitude of relaxation transient, duration of early slow force decline - measured from onset of solution change to the beginning of the exponential force decay, the rate constant of the final exponential phase of force decline (kREL, EXP).

NRVM Transfection

Neonatal rat ventricular cardiomyocytes (NRVMs) were prepared from neonatal rat hearts as previously described (91). Isolated cells (~2.5 x 10^6) were transfected with the Amaxa Rat Cardiomyocyte Neo Nucleofector Kit and DNA according to the manufacturer's protocol and were plated on 1% gelatin-coated glass coverslips. Cells were imaged approximately 72 hours after transfection and imaged by confocal microscopy.

Data & Statistical Analyses

Data are presented as mean ± SEM. Differences between groups were evaluated for statistical significance using Student's two-tailed t test (comparison between two groups) or one-way ANOVA (comparison among more than two groups) followed by Tukey's

post-hoc test for pairwise comparisons. P values less than 0.05 were considered significant unless otherwise noted.

CHAPTER III

Laing Distal Myopathy R1500P Mutation Alters Sarcomeric Mechanics via Faster Cross-bridge Detachment

Abstract

Laing distal myopathy (MPD1) is a progressive disorder initially characterized by weakness of selective distal muscles. Since proline substitutions mapped in the coiled-coil region of the β-myosin (MYH7) gene are the most common causes of MPD1, we developed a mouse model expressing the mutant R1500P myosin. Here we show that transgenic mice present histological phenotypes often found in human biopsies such as muscle fiber hypotrophy, mitochondrial abnormalities and ultra-structural changes in the sarcoplasmic reticulum (SR). By subjecting the transgenic mice to voluntary wheel running and muscle strength assays, we find that both endurance performance and force are negatively affected. Moreover, ex-vivo contractility experiments carried out on EDL muscle indicate altered kinetics and higher fatigability. Lastly, single myofibril analysis reveals that mutant residency in the thick filament adversely impacts sarcomere mechanics by significantly increasing the rate constant of the first part of the relaxation phase, which corresponds to cross-bridge detachment from actin. Thus, proline rod mutations do not primarily affect myosin assembly as originally proposed, but rather influence the actomyosin mechano-chemical cycle and ultimately, muscle tension generation. These studies provide first evidence of the molecular mechanisms underlying MPD1 and lay the groundwork for the development of future MPD1 therapeutic interventions.

Significance Statement

Laing distal myopathy is a disorder that affects distal skeletal muscles. The disease is characterized by progressive muscle weakness that can appear in childhood as well as later in life. Laing distal myopathy is caused by proline mutations in the *MYH7* gene, which encodes the heart/skeletal muscle motor β-myosin. Since limited information is available about the pathogenic mechanisms triggered by the MYH7 mutations, we have developed the first transgenic mouse model for the disease expressing the R1500P substitution. The findings presented in this study identify the molecular impact of the mutation on the activity of the contractile machinery and provide an important groundwork for developing new therapeutic strategies.

Introduction

Laing distal myopathy (MPD1) is an autosomal dominant disease with variable timing of disease onset that spans from birth into adulthood (53). MPD1 affects skeletal muscle function in a progressive manner: clinically, symptoms begin with weakness in the lower leg anterior compartment that impacts ankle and great toe dorsiflexion (92, 93). Contrary to many other muscle disorders, pathologic findings in muscle biopsies from MPD1 patients are often inconsistent (53).

MPD1-causing mutations have been mapped to the *MYH7* gene that encodes the β-myosin heavy chain, the primary myosin motor expressed in both human heart and in type I, slow skeletal muscle fibers (59). Unexpectedly, only a small number of MPD1 patients also develop a cardiomyopathy, despite higher levels of β-myosin expression in the heart (45, 53, 55–57). MYH7 is a hexameric molecule comprised of a pair of heavy chains and two pairs of non-identical light chains. ~400 pathogenic mutations causing cardiac and distal myopathies have been identified in both the N-terminal motor domain as well as in the coiled-coil rod region of MYH7 (http://www.hgmd.cf.ac.uk/ac/index.php). The majority of MPD1 mutations are located in the light meromyosin (LMM) domain corresponding to the C-terminal third of the rod that controls assembly of myosin into the thick filaments (56, 60, 61). However, a small number of them are also located in the motor domain (62, 63). MPD1 mutations are primarily codon deletions and missense mutations that introduce a proline residue (56, 60, 61). Both of these genetic defects are predicted to negatively impact the structure of the myosin coiled-coil structure (64). For example, proline residues found in α-helices induce a ~26-degree kink that could locally unwind the myosin coiled-coil (64).

The biological effects of a subset of MPD1 mutations have been characterized in both non-muscle and muscle cells (67, 94). Muscle cell-based studies have shown that proline rod mutations do not impair incorporation of the mutant myosins into the sarcomere (12) and therefore do not block formation of the rod coiled-coil structure as originally proposed (60). However, they can trigger myosin cytoplasmic aggregates (12) or cause aberrant myosin packing in thick filaments (66). A progressive dominant hind/fore limb myopathy resembling MPD1 but associated with high frequency of myocardial infarctions has been reported in pigs (95). In this model, sequence analysis revealed an in-frame insertion of two residues (alanine, proline) in MYH7 exon 30; muscle fiber degeneration and regeneration and interstitial fibrosis were also observed. More recently, to characterize the molecular mechanisms of the MPD1-causing mutation L1729del, a *Drosophila melanogaster* model for MPD1 was established (68). By recapitulating some of the morphological muscle defects such as sarcomeric disorganization and myofibril damage observed in patients, this study provided new insight into the pathogenesis of the disease. However, how MDP1 rod mutations act in the mammalian muscle environment remains unclear and understudied. In fact, while numerous genetic mouse models have been developed for studying MYH7 motor domain mutations that cause hypertrophic or dilated cardiomyopathy (49), no mammalian genetic models have yet been reported for examining the effects of myopathy-causing mutations in the rod domain. To fill this research gap, we created the first MPD1 mouse model expressing the R1500P rod mutation identified in a previous study (60). Our data reveal that expression of the mutant myosin affects both muscle histological structure and performance. Transgenic mice show decreased muscle strength and endurance, as well as decreased resistance to fatigue. Remarkably, we also found that the presence of the R1500P rod mutation weakens acto-myosin binding by affecting

cross-bridge detachment rate. Since the phenotype of the transgenic mice closely mimics MDP1, we believe that our animal model will be a useful platform for testing and developing future therapeutic interventions for MPD1.

Results

Generation and characterization of R1500P mice

To create a mouse model for MPD1, we generated mice expressing the β-myosin R1500P mutation under the control of the well-characterized muscle creatine kinase (MCK) promoter that restricts transgene expression to fast skeletal muscle fibers only. We followed this strategy to circumvent the much lower abundance of slow/Type I fibers in the mouse compared to human (Figure 3.1A), and therefore increase the opportunity to reveal a muscle phenotype. As previously reported (78), we tracked expression of the transgene by tagging the C-terminal end of the mouse rod domain, which is 99% identical to the human homolog, with a myc-tag epitope. As a control, mice expressing myc-tagged WT β-MyHC were also created (Figure 3.1A). We obtained 3 transgenic lines for each group, all expressing similar amounts of WT and mutant transgene protein (Supplementary Figure 3.1A). Moreover, we found that in tibialis anterior (TA) muscle, their expression levels are ~35% of total myosin. (Figure 3.1B). In agreement with the MCK promoter specificity (79), we did not detect transgene expression in any muscles that normally express detectable amounts of Type I/ slow myosin such as soleus and heart (Supplementary Figure 3.1B).

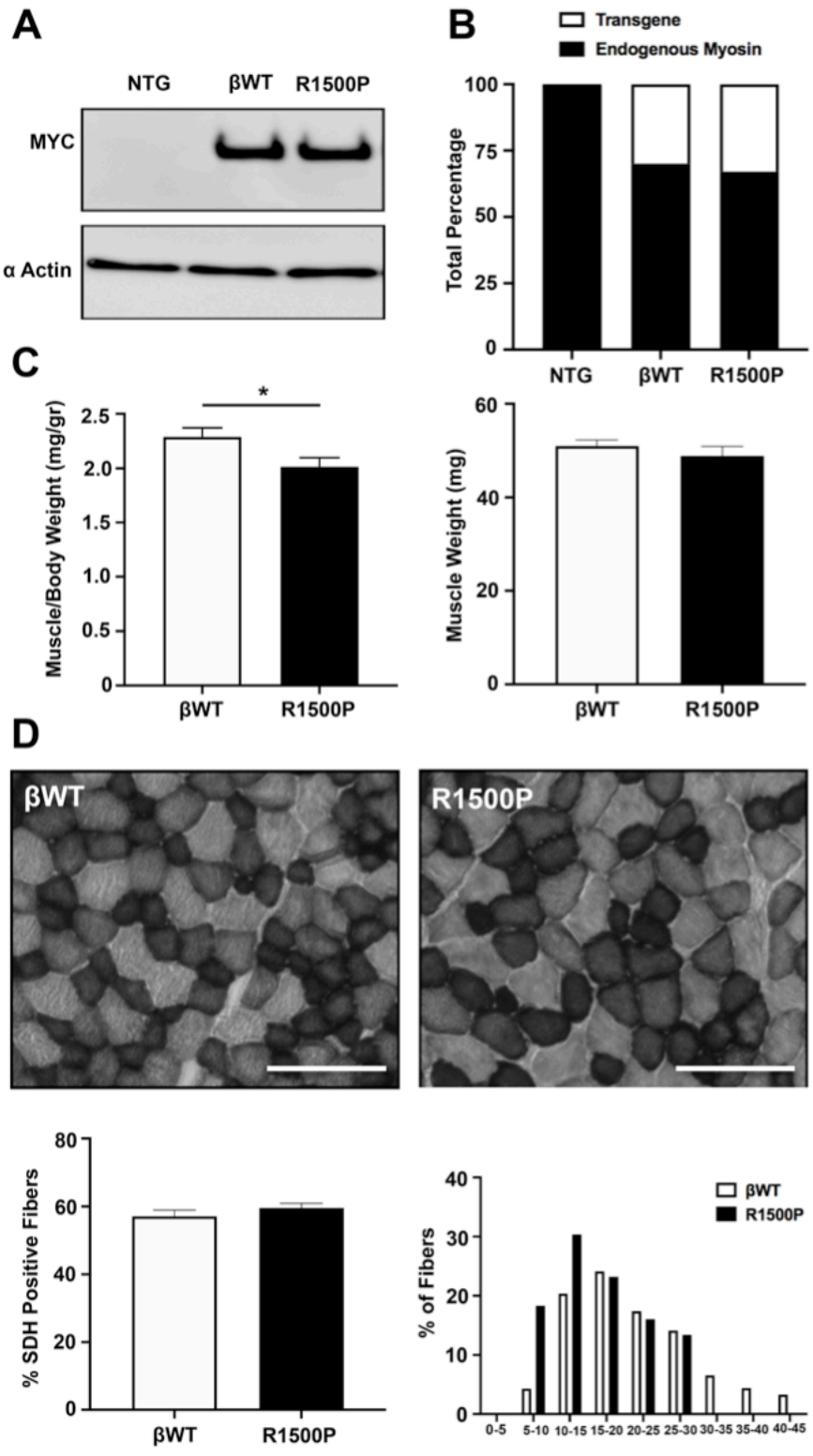
A
NTG
βWT
R1500P
MYC
α Actin
B
Transgene
Endogenous Myosin
Total Percentage
100
75
50
25
0
NTG
βWT
R1500P
C
Muscle/Body Weight (mg/gr)
2.5
2.0
1.5
1.0
0.5
0
*
βWT
R1500P
Muscle Weight (mg)
60
40
20
0
βWT
R1500P
D
βWT
R1500P
% SDH Positive Fibers
80
60
40
20
0
βWT
R1500P
% of Fibers
40
30
20
10
0
βWT
R1500P
0-5
5-10
10-15
15-20
20-25
25-30
30-35
35-40
40-45

Fig. 1. Characterization of transgenic muscles expressing the myosin mutant R1500P. (*A*) Representative Western blot analysis of total protein extracts purified from tibialis anterior (TA) and probed with myc and α-sarcomeric actin (used as a loading control) antibodies. NTG: non transgenic animals; βWT: transgenic animal expressing WT MYH7; R1500P: transgenic animal expressing mutant MYH7. (*B*) The comparative quantification between the R1500P mutant and the endogenous WT myosin was determined by defining total myc and total myosin using myc and F59 antibodies respectively. (*C*) Average muscle/body weight ratio (Left Panel) and muscle weight (Right Panel) of tibialis anterior muscles isolated from 6-10-month-old βWT and R1500P mice (n =20/group). (*D*) Representative SDH activity of cross-sections of TA muscles isolated from βWT (Top Left Panel) and R1500P mice (Top Right Panel). Bottom Left Panel: SDH positive fibers quantification; Bottom Right Panel: fiber size quantification; x-axis indicates muscle fiber area, expressed in um^2. Bar(s) corresponds to 200 um.
All data are expressed as mean +/- SEM. *p < 0.05, ****p < 0.0001 by two-tailed unpaired t-test with Welch's correction.

Characteristic MPD1 histopathology is present in R1500P muscles

Histological features associated with MPD1 are frequently variable and can include: i) change in muscle fiber size with type I hypotrophy, ii) co-expression of slow and fast myosins, iii) core/minicore structures, iv) mitochondrial abnormalities, and v) muscle necrosis and regeneration (53, 58). Hence, we next determined whether the expression of the R1500P mutant in our mouse model induces some of the pathological phenotypes observed in human muscles. We found that while expression of the R1500P mutant did not change the whole muscle weight of measured fast-type muscles, it significantly decreased the muscle/body weight ratio when compared to the βWT transgenic control (Figure 3.1C). Histological analysis of WT and R1500P TA muscle enzymatically stained for the mitochondrial enzyme succinate dehydrogenase (SDH) showed no significant difference in the percentage of positive fibers (Figure 3.1D).

However, while the proportion of fast versus slow muscle fibers was unchanged, measurement of fiber cross-sectional area showed that R1500P muscle had a higher proportion of smaller muscle fibers than the βWT control (Figure 3.1D). Thus, fiber hypotrophy could account for the observed decrease in muscle/body weight. To measure the level of expression of the different myosin heavy chain isoforms in TA muscle, we carried out quantitative real-time PCR (qRT-PCR). We found that RNA for both the slowest and fastest myosin isoforms (Myh7 and Myh4 respectively) were upregulated by R1500P mutant expression, while the RNA level of the intermediate skeletal myosin isoforms Myh2 and Myh1 were not affected (Supplementary Figure 3.2A). However, while Myh4 RNA was upregulated, the same was not observed at the protein level (Supplementary Figure 3.2B). To determine if expression of the R1500P mutant myosin led to sarcomere disorganization, we next complemented these studies by analyzing TA muscle ultrastructure with transmission electron microscopy (TEM). This analysis revealed that the integrity of the major sarcomeric components was not affected. However, ultrastructural changes in the sarcoplasmic reticulum (SR), t-tubules, and mitochondria were observed in the R1500P animals. While WT muscles showed the normal pattern of tightly wound SR networks with accompanying t-tubule triads, R1500P muscles had distended, irregular, and enlarged SR with the t-tubules having a variety of abnormalities ranging from mild to severe dilation of the triad structure (Figure 3.2A, 3.2B, Supplementary Figure 3.2C). Furthermore, as confirmed by quantification of mitochondrial DNA content, the number of mitochondria was also decreased (Figure

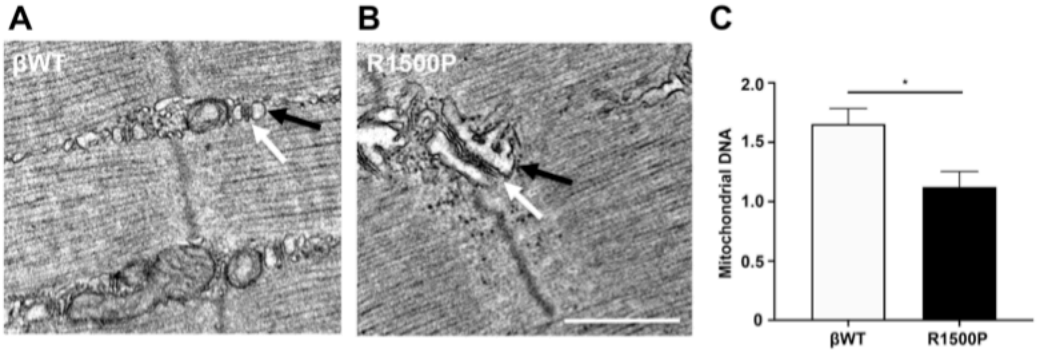

Figure 3.2. Electron microscopy analysis of R1500P TA muscles shows no morphological changes in the structure of the sarcomeres but reveals sarcoplasmic reticulum (SR) and t-tubule disorganization associated with a decreased number of mitochondria. (*A, B)* Electron microphotographs of longitudinal sections of TA muscles isolated from 8-month-old WT and R1500P mice. While expression of βWT myosin does not affect the structure of t-tubule triads and SR network (*A*), the presence of the R1500P mutant induces dilation of the t-tubules accompanied by distension and enlargement of the SR (*B*). *(C)* Relative mitochondrial DNA content of CO1 normalized to 18S rRNA. Arrows denote triad structures formed by t-tubules (white arrow) and two portions of the SR (black arrows) normally located between sarcomeres and close to the Z-line (*A*). Bar(s) corresponds to 742 nm.
All data are expressed as mean +/- SEM. *$p < 0.05$ by two-tailed unpaired t-test with Welch's correction.

3.2C). Taken together, these results demonstrate that a number of the histological hallmarks that are often identified in patients with MPD1 are also present in our transgenic mouse model. Moreover, they provide evidence that the SR structure and/or function could also be altered by the expression of the R1500P mutant myosin.

The presence of the R1500P mutation activates genes involved in skeletal muscle ER stress and the unfolded protein response (UPR)

Changes and/or disruptions to the ultrastructure of skeletal muscle can cause endoplasmic reticulum (ER) stress, which affects proper ER function by increasing the amount of misfolded/unfolded proteins in the ER lumen (97). As a result, a homeostatic signaling pathway, called Unfolded Protein Response (UPR) is activated. UPR inhibits

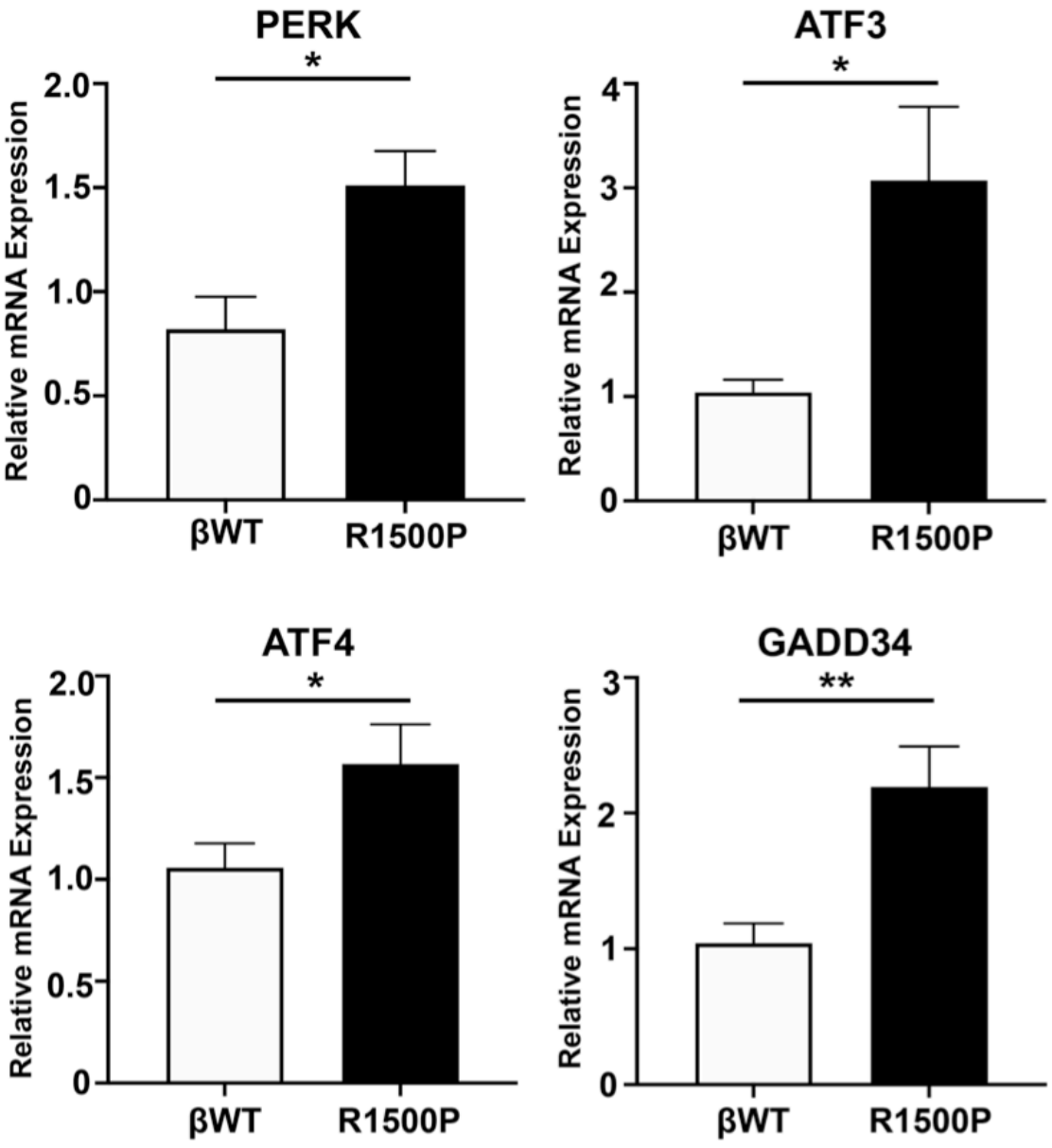

Figure 3.3. Expression of the myosin mutant R1500P activates genes in the unfolded protein response (UPR) pathway. mRNA induction of UPR genes was measured by qRT-PCR. Total RNA was purified from TA muscles of 6-8-month-old βWT and R1500P transgenic mice. Reactions were normalized to 18S rRNA.
Data are expressed as mean +/- SEM. *$p < 0.05$, **$p < 0.01$ by two-tailed unpaired t-test with Welch's correction.

protein synthesis, increases ER concentration of chaperones, and ultimately triggers apoptosis (23). Since recent evidence has indicated that UPR is upregulated in a variety of myopathies (101–104), we measured the RNA levels of members of the PERK pathway, which is one of the major UPR transducers and has previously been shown to be activated in muscular dystrophy (101). In TA muscle of R1500P mice, we found significant upregulation of PERK and downstream members of the pathway including ATF4, ATF3, and GADD34 (Figure 3.3). Other related members of the PERK pathway, such as CHOP were, however, unaffected by the presence of the R1500P mutation (data not shown). Thus, in skeletal muscle, heightened activation of genes involved in the UPR pathways may contribute to the development of the MPD1 phenotype.

Muscle fitness and strength are decreased in R1500P mice

To determine whether the R1500P mutation hinders the biochemical mechanics of muscle contraction, we first measured exercise tolerance and fitness in βWT and R1500P mice using a fully automated tracking system to monitor voluntary wheel running. This analysis showed that both the running speed and total running distance over a 28-day period was significantly reduced in 3-, 8- and 12-month-old male R1500P mice when compared to their βWT counterparts (Figure 3.4A). Consistent with these results, muscle strength analyses including a four-limb hanging test and grip strength measurements were impaired with decreased average hang time and a significant reduction in force output in R1500P animals (Figure 3.4B, 3.4C). Thus, as seen in MPD1 patients, the expression of the R1500P mutant in our model affects muscle performance and strength.

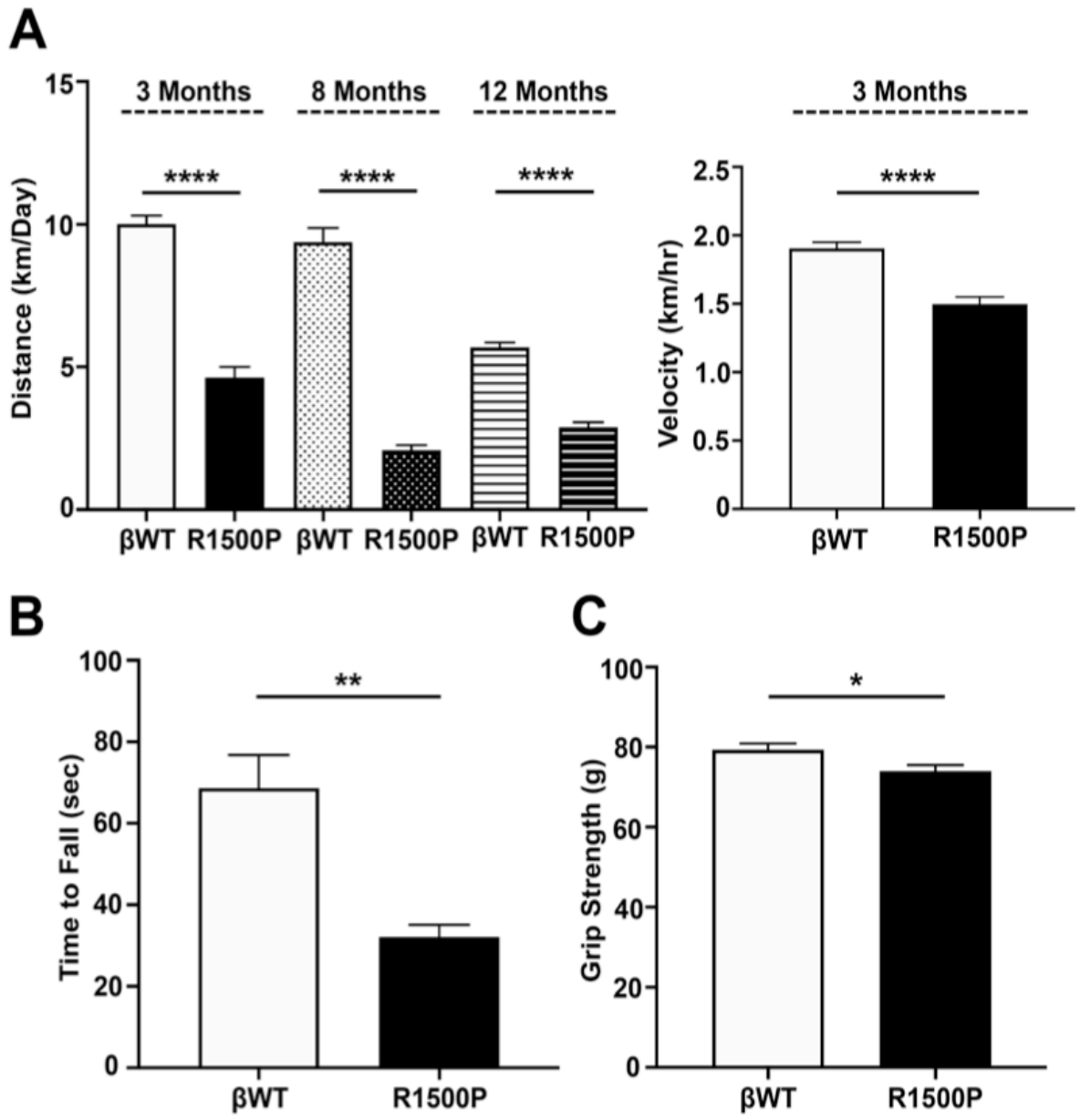

Figure 3.4. Muscle endurance and force are compromised in R1500P transgenic mice.
To assess muscle endurance male βWT and R1500P transgenic mice were subjected to voluntary wheel running over 28 days. Average running distance and average speed (*A*, left and right panels respectively) are expressed in km/day and km/hr respectively; the age of the mouse groups assayed is reported on the top of each graph (n = 10-12/group). Four-limb hanging test, which measures sustained muscle tension, which counteracts animal gravitational force (*C*) and grip test (*D*) were used to determine muscle strength deficits. For each animal the hanging time to the wire mesh screen was calculated after three trials (n = 6/group, 8-month-old mice); measurements of forelimb grip strength were carried out with a computerized grip strength meter (n = 6/group, 8-month-old animals).
Data are expressed as mean +/- SEM. *$p < 0.05$, **$p < 0.01$, ****$p < 0.0001$ by two-tailed unpaired t-test with Welch's correction.

***Ex-vivo* contractility assay shows altered R1500P muscle contractility**

Since the parameters of muscle contractility, force, fatigability and contractile kinetics can be measured in isolated muscles, we next assessed the *ex-vivo* properties of the extensor digitorum longus (EDL) muscles expressing βWT or R1500P myosins. EDL muscles were used instead of the TA since the protocol requires intact muscle-tendon complexes (80). As a control, the properties of the slow-twitch soleus muscle were also analyzed. Measurements of tetanic and twitch force were performed after determining the optimal muscle length. While specific tetanic force was not affected by the presence of the R1500P mutation (Figure 3.5A), specific twitch force was significantly increased in R1500P EDL muscles while the twitch to tetanus force ratio was significantly decreased (Figure 3.5B, 3.5C). In contrast, the activity of WT and R1500P soleus muscles, which do not express the transgene, did not show any functional difference (Supplementary Figure 3.2 A-D). Figure 3.5D shows the force versus frequency relationship for EDL muscles obtained from WT and R1500P EDL muscles. In agreement with the observed decreased twitch/tetanus ratio, the R1500P curve is shifted to the right (downward). Notably, this phenotype, previously characterized as low-frequency fatigue, appears to be linked to altered calcium release (105). We next determined muscle fatigue by challenging the muscles with high frequency stimuli (100 Hz), which induced sustained muscle contraction; as the muscle relaxed over time, we measured the force output as an indicator of fatigue. The measurements obtained showed that the percentage of peak tetanic force dropped more quickly for R1500P muscle (Figure 3.5E) suggesting that in addition to a drop in force production, the muscles expressing the mutant myosin have decreased resistance to fatigue.

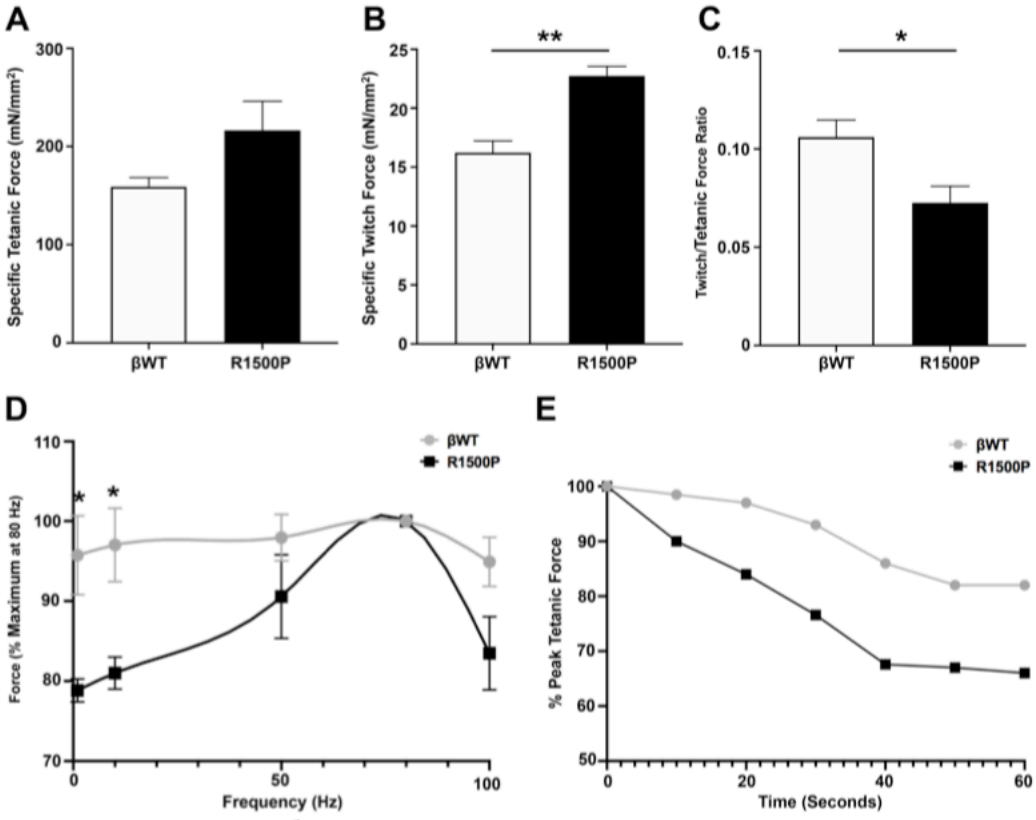

Figure 3.5. Expression of the myosin mutant R1500P impairs isolated skeletal muscle performance. EDL muscles isolated from 8-month-old βWT and R1500P mice were subjected to *ex-vivo* contractility assay. Measurement and comparison of basal specific twitch force (*A*), specific tetanic force (*B*), their ratio (*C*), as well as force vs frequency (*D*) and fatigue (*E*) tests are reported. Stimulatory trains of varying frequency (1-100 Hz) were used to generate force-frequency curves. Tetanic force was achieved using 100 Hz.
(*A)* through (*D)*: βWT, n = 5/group; R1500P, n = 3/group. (*E)*: βWT, R1500P n = 1/group. Data are expressed as mean +/- SEM. *$p < 0.05$, **$p < 0.01$ by two-tailed unpaired t-test with Welch's correction.

The R1500P mutation affects myofibril relaxation

To widen our biochemical and molecular characterization on the contractile properties of muscles expressing the R1500P mutation, we then analyzed force generation and relaxation kinetics of isolated muscle fibers from TA muscle. Mounted myofibrils were activated and relaxed by rapidly switching between two flowing solutions of pCa 4.5 and pCa 9.0. While activation is described by a single exponential function with constant rate k_{ACT}, relaxation of myofibrils follows a biphasic state: an initial slow linear phase followed by a faster exponential decay. The rate and duration of the slow phase, which is mainly determined by thin filament inactivation and cross-bridge detachment, is defined by slow $k_{REL,\ LIN}$ and t_{REL} respectively. The final exponential phase of force decline is instead defined by the rate constant fast $k_{REL,\ EXP}$.

Although we did not detect changes in any mechanical parameters, which includes resting, maximal tension, and activation kinetics, k_{ACT} or $k_{TR.}$ (Supplementary Figure 3.5 A-D), we nevertheless observed that the rate of slow phase relaxation ($k_{REL,LIN}$) was significantly increased in R1500P myofibrils when compared to WT controls (Figure 3.6B), whereas the duration of slow phase relaxation (t_{REL}) was significantly decreased (Figure 3.6C). In contrast, the rate of the rapid exponential phase of relaxation ($k_{REL,EXP}$) was unchanged (Figure 3.6D). No difference in activation or relaxation was identified in myofibrils purified from WT and R1500P soleus muscle (Supplementary Figure 3.5 A-E). The faster cross-bridge detachment observed in these experiments indicates that the proline substitution studied here, could act on muscle function by affecting proper acto-myosin binding.

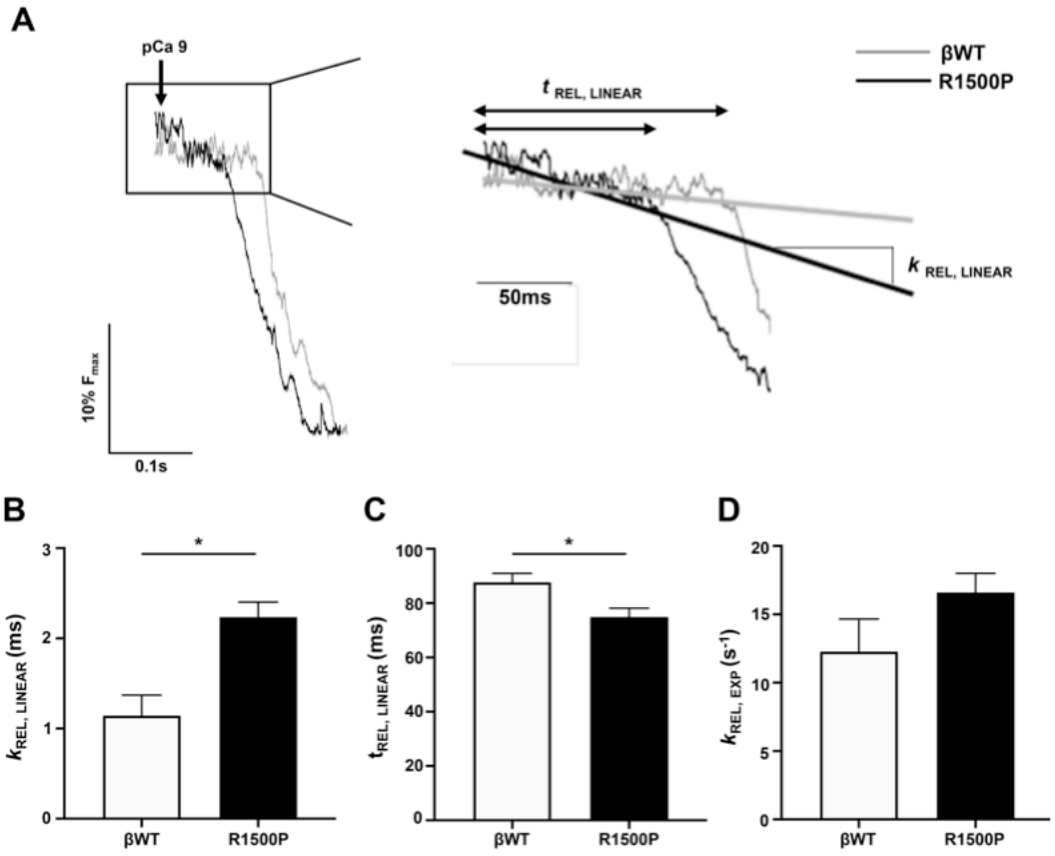

Figure 3.6. Myofibrils containing the myosin mutant R1500P show faster crossbridge detachment under isometric conditions. Representative trace of myofibril linear and exponential phase relaxation from myofibrils isolated from TA of R1500P mutants and βWT controls. (*A*). Rate constant ($k_{REL, LINEAR}$) and duration ($t_{REL, LINEAR}$) of the early linear phase of relaxation (*B*; *C*) and rate constant of the final exponential phase of force decline ($k_{REL, EXP}$) measured from βWT and R1500P myofibrils (*D*). Myofibrils were isolated from TA muscles of 6-month-old βWT and R1500P mice.

Data are expressed as mean +/- SEM of 6-8 myofibrils/tibialis anterior muscle. βWT, n = 3/group; R1500P, n = 5/group. *p < 0.05 by two-tailed unpaired t-test with Welch's correction.

Discussion

In this study we present characterization of the first mouse model for MPD1 caused by the MYH7 R1500P mutation. By showing that both the histological and functional phenotypes often found in MPD1 patients match the ones present in our transgenic animals, our system closely models the human disease and reveals novel insights into the molecular mechanisms of MPD1. About 60% of the MPD1 missense mutations are proline substitutions found randomly distributed in the seven positions of the MYH7 myosin coiled-coil heptad repeat (http://www.hgmd.cf.ac.uk/ac/index.php). Paradoxically, the R1500P mutation, which is located in the *f* position of the heptad repeat, causes MDP1, while the homologous R1500W substitution causes dilated cardiomyopathy without distal myopathy (57, 106). The majority of non-proline substitutions are associated with cardiomyopathy and only a small number of E to K charge reversals located towards the end of the coiled-coil elicit a mixed cardiac and skeletal phenotype (45). Since all proline rod substitutions result in MPD1, they must alter the local geometry of the coiled-coil through a common structural signature that induces distal myopathy. Thus, we believe that our transgenic model is phenotypically linked not only to the R1500P mutation but could recapitulate the pathological steps initiated by proline mutations located in different positions of the myosin rod.

Patients diagnosed with MPD1 present with specific clinical but variable muscle pathological phenotypes with no representative histological hallmark that can lead to a definitive diagnosis of the disease. Individuals carrying the R1500P mutation show fiber type disproportion consistent with hypotrophy of slow-type muscle fibers, but variable predominance of Type 1 muscle fibers (53, 58). Unfortunately, ultrastructural analysis of

MPD1 muscles has been carried out only in patients having the K1729del mutation (53). In the latter report, the most frequent finding (the only abnormality found in 2 biopsies) was variation in muscle fiber size, with predominant small type 1 and large type 2 fibers. However, dilated triads or their depletion, confluent T-tubules and mitochondrial abnormalities were also observed. Regardless of the etiology, T-tubule abnormalities are also frequently found in failing cardiomyocytes. Whether changes in their architecture are the main cause of disease or only induce/aggravate the cardiac phenotype remains to be determined (107). However, imbalance in calcium levels triggers endoplasmic reticulum (ER) stress, which results in the activation of two different cellular pathways: the unfolded protein response (UPR) and the ER overload response (EOR) (97). Therefore, we believe that the activation of the UPR signaling pathway found in the transgenic R1500P muscles (Figure 3) is secondary to altered calcium levels associated with deterioration in T-tubule function more than the formation of myosin cytoplasmic aggregates (67), which activate ER stress, but were not detected in the R1500P muscle sections. Thus, based on the similarity with some of the human findings reported above, our data indicate that at the histological level, our transgenic mouse model appears to mimic the muscle phenotype observed in patients.

It has been suggested that proline mutations incorporated in the sarcomere cause MDP1 by altering the proper packing of the myosin rod; as a result, both the turnover and stability of the sarcomere could be affected (65–67). While showing that structural integrity observed in sarcomeres containing the R1500P myosin mutant does not necessarily equate with their functional integrity, the mechanical parameters measured from skinned myofibrils broaden our understanding of the molecular basis of the beginning and progression of MPD1. Since myofibril experiments measure force generation during the sarcomere contraction-relaxation cycle in the absence of the other

cellular muscle components, they directly probe defects in myosin cross-bridge cycling (108). This analysis revealed that incorporation of R1500P myosin mutant in the thick filaments alters relaxation: while the rate of the slow phase relaxation ($k_{REL,LIN}$) was almost two-fold faster (1.95X), its duration (t_{REL}) was significantly shorter (0.85X). Since the $k_{REL,LIN}$ measured in isometric conditions reflects the rate of actin-myosin detachment (cross-bridges leaving force-generating states) (82, 109), we believe that the local rod structural changes created by the R1500P proline mutation affect the cross-bridge cycling of the thick filament. In this unique molecular framework, which contains ~300 myosin molecules, the negative effects of a single missense mutation can, in fact, become additively detrimental and alter thick filament geometry/stability. These last two pathological conditions can affect the tension generation process by impacting accurate docking and cross-bridge turnover. Moreover, the faster cross-bridge actin separation observed here suggests that during contractile activity, sarcomeres containing the R1500P mutant could require higher energetic cost (tension over ATPase activity ratio) to generate and maintain adequate muscle tension (110). The data also cast light on the pathological mechanisms operating at the sarcomeric level that could be responsible for i) the drop in force production and decreased resistance to fatigue seen in the *ex-vivo* experiments (Figure 5) and ii) muscle motor impairment exposed by the running and grip strength assays (Figure 4). Two other studies characterized the mechanical performance of myofibrils purified from patients with MYH7 mutations. One report showed faster tension generation as well as faster relaxation ($k_{REL,EXP}$, which is mainly driven by inter-sarcomeric dynamics and lead to broad sarcomere lengthening) in myofibrils containing the HCM mutation R403Q (111). A second investigation on the effect of the DCM rod mutation E1426K found higher k_{TR}, shorter t_{REL}, and faster $k_{REL,EXP}$ (112). These results suggest that mutations associated with HCM/DCM or skeletal myopathies could have

distinct negative effects on the different mechanical phases that occur during sarcomere contraction. Thus, it might be possible that, irrespective of their rod location and heptad position, the common structural distortion introduced by proline mutations in the myosin rod, also results in a common and unique pathological effect on sarcomeric cross-bridge kinetics. Taken together, the findings presented here report the development and validation of the first animal model for studying the pathogenesis of MPD1 and for developing and testing the efficacy of different types of molecular therapies. Importantly, they also provide for the first time the potential molecular basis for the disease.

Materials and Methods

Animal Care

All animal experiments were performed using protocols approved by University of Colorado Institutional Animal Care and Use Committees (IACUC). Animals were housed under standard conditions in a partial barrier facility and received access to water and chow *ad libitum*. For sample collection, animals were sedated using 1-4% inhaled isoflurane and sacrificed by cervical dislocation. All data shown is from male mice.

Western Blotting

Protein lysates were prepared by homogenizing hindlimb muscle tissue in myosin extraction buffer (0.3M NaCl, 0.1M NaH_2PO_4, 0.05M Na_2HPO_4, 0.001M $MgCl_2.6H_2O$, 0.01M EDTA) following standard procedures. The antibodies used were against Myc-Tag (9B11) (1:10000, Cell Signaling Technology, #2276), F59 (1:50), BF-F3 (MYH4, 1:20), and α-sarcomeric actin (1:2000). All blots were imaged using the ImageQuant LAS 4000 (GE

Healthcare Bio-Sciences, Pittsburg, PA) system and analyzed with the ImageQuant software and/or with ImageJ.

RNA Isolation & Quantification

Total RNA was purified from hindlimb muscles using TRI Reagent (Ambion) according to manufacturer's protocol. cDNA was synthesized using SuperScript III reverse transcriptase (Invitrogen) and random hexamer primers. Gene expression was determined by qRT-PCR using SYBR Green dye (Invitrogen) and gene specific primer sets. All genes were normalized to 18S rRNA expression. Data were collected and analyzed using Bio-Rad CFX Real-Time PCR system.

Histology (Succinate Dehydrogenase Staining)

Tibialis anterior muscles were snap frozen in isopentane/liquid N_2, cryo-sectioned, and stained for enzymatic activities using standard procedures. The stained fibers were counted and their percentage of total number of fibers was calculated (150–200 total fibers/image, 3 images/mouse, 2 mice/genotype). Cross sectional area was determined using ImageJ.

Transmission Electron Microscopy

Skeletal muscle was dissected and immersed in 2.5% glutaraldehyde and 2% paraformaldehyde in 0.1 M cacodylate buffer at pH 7.4 for a minimum of 24 hours at 4°C. For processing, the tissue was rinsed in 100 mM cacodylate buffer and then immersed in 1% osmium and 1.5% potassium ferrocyanide for 15 min. Next, the tissue was rinsed five times in cacodylate buffer, immersed in 1% osmium for 1 hour, and then rinsed again five times for 2 min each in cacodylate buffer and two times briefly in water. The tissue was

stained en bloc with 2% uranyl acetate for 1 hour before it was transferred to graded ethanols (50, 70, 90, and 100%) for 15 minutes each. Finally, the tissue was transferred through propylene oxide at room temperature and then embedded in LX112 and cured for 48 h at 60^{o}C in an oven. Ultra-thin sections (55 nm) were cut on a Reichert Ultracut S from a small trapezoid positioned over the tissue and were picked up on Formvar-coated slot grids or copper mesh grids (EMS). Sections were imaged on a FEI Tecnai G2 transmission electron microscope (Hillsboro, OR) with an AMT digital camera (Woburn, MA).

Functional Phenotypic Measurements

Voluntary Wheel Running

Male mice were subjected to voluntary wheel running for a period of 28 days at the age of 3 months, 8 months, and 12 months. Mice were housed individually in a large cage with a running wheel. Exercise time, velocity, and distance were recorded daily for each animal.

Grip Strength

Forelimb grip strength was measured with a grip strength meter. The mice were first acclimated to the apparatus for approximately 5 min. Individual mice were then allowed to grab the bar while being held from the tip of their tail. The mouse was gently pulled away from the grip bar. When the mouse could no longer grasp the bar, the reading was recorded. Protocol was repeated five times with at least 30 sec rest between trials. The highest three values were averaged to obtain the absolute grip strength.

Four Limb Hanging Test

Male mice were placed in the center of a wire mesh screen, a timer was started, and the screen was rotated to an inverted position with the mouse's head declining first. The

screen was held above a padded surface. Either the time when the mouse falls was noted, or the mouse was removed when the criterion time of 60 sec was reached.

Ex-Vivo Contractility Assay

Mice were euthanized according to NIH guidelines and IACUC institutional animal protocols. Extensor digitorum longus (EDL) was carefully dissected in total from the ligamentary attachment at the lateral condyle of the tibia to the insertion region. The muscle was transferred to a dish containing ice-cold isotonic physiologic salt solution (Tyrode's buffer (mM): NaCl 118, KCl 4, $MgSO_4$ 1.2, $NaHCO_3$ 25, NaH_2PO_4 1.2, glucose 10 and $CaCl_2$ 2.5) bubbled with 95% O2/5% CO2 to maintain a pH of 7.4. The soleus was identified after removing the gastrocnemius muscle and was removed by cutting the ligaments connecting to the proximal half of the posterior tibia to the insertion, where the calcaneal tendon was cut and the muscle was placed into ice-cold Tyrode's buffer. Muscles were mounted vertically in individual tissue bath chambers and maintained at 37° C. Muscles were stretched and optimal length was set for each muscle. Stimulatory trains of varying frequency (1-100 Hz) were used to generate force-frequency curves. Tetanic force was achieved in all muscles using 100 Hz.

Myofibril Isolation

Myofibrils were isolated from flash frozen soleus and tibialis anterior as described (85, 86). A small section of muscle was cut into thin slices and bathed in 0.05% Triton X-100 in Linke's solution (132mM NaCl, 5mM KCl, 1mM $MgCl_2$, 10mM Tris, 5mM EGTA, 1mM NaN_3, pH 7.1) with protease inhibitor cocktail (10 μM leupeptin, 5 μM pepstatin, 200 μM phenyl-methylsuphonylfluoride, 10 μM E64, 500 μM NaN_3, 2 mM dithioerythritol) overnight at 4°C overnight. Skinned tissue was washed three times in rigor solution

(50mM Tris, 100mM KCl, 2mM $MgCl_2$, 1mM EGTA, pH 7.0) and resuspended in bath solution with protease inhibitors (pCa 9.0; 100mM Na_2EGTA; 1M potassium propionate; 100mM Na_2SO_4; 1M MOPS; 1M $MgCl_2$; 6.7mM ATP; and 1mM creatine phosphate; pH 7.0) and homogenized at medium speed for 10 seconds three times.

Myofibril Mechanics

Myofibrils mechanical parameters were measured as described (86–88). Myofibrils were placed on a glass coverslip in relaxing solution at 15°C and then a small bundle of myofibrils were mounted on two microtools. One microtool was attached to a motor that produces rapid length changes (Mad City Labs) and the second microtool was a calibrated cantilevered force probe (5.8 μm/μN; frequency response 2-5 KHz). Myofibril length was set at 5-10% above slack length and average sarcomere length and myofibril diameter were measured using ImageJ. Mounted myofibrils were activated and relaxed by rapidly translating the interface between two streams of solutions of pCa 4.5 and pCa 9.0 (88, 89). Data was collected and analyzed using customized LabView software. Measured mechanical and kinetic parameters were defined as follows: resting tension (mN/mm^2) – myofibril basal tension in fully relaxing condition; maximal tension (mN/mm^2) – maximal tension generated at full calcium activation (pCa 4.5); the rate constant of tension development following maximal calcium activation (k_{ACT}); the rate constant of tension redevelopment following a release-restretch applied to the activated myofibril (k_{TR}) (90); rate constant of early slow force decline ($k_{REL,\ LIN}$) - the slope of the linear regression normalized to the amplitude of relaxation transient, duration of early slow force decline - measured from onset of solution change to the beginning of the exponential force decay, the rate constant of the final exponential phase of force decline ($k_{REL,\ EXP}$).

Data & Statistical Analyses

Data are presented as mean ± SEM. Differences between groups were evaluated for statistical significance using Student's two-tailed t test (two groups) or one-way ANOVA (more than two groups) followed by Tukey's post-hoc test for pairwise comparisons. *P* values less than 0.05 were considered significant unless otherwise noted.

Supplemental Information

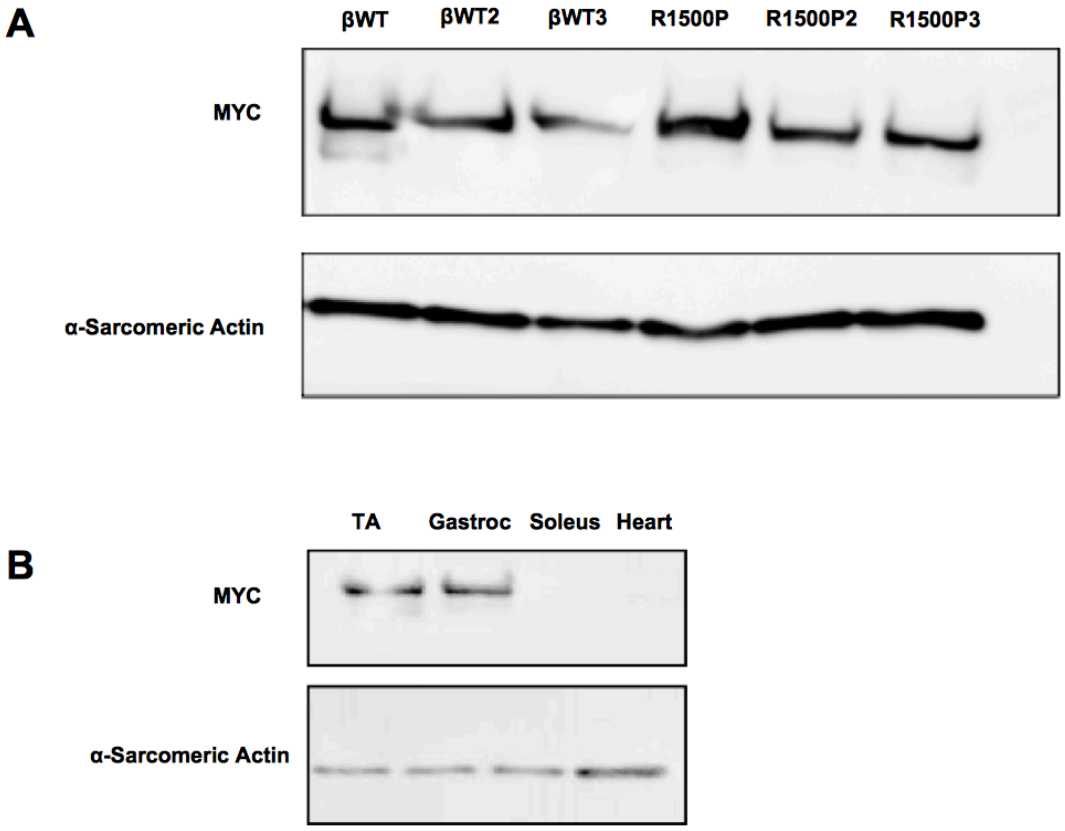

Supplemental Figure 3.1. Transgene expression in βWT and R1500P transgenic mice.
(*A*) Representative Western blot analysis of total protein extracts purified from tibialis anterior (TA) and probed with myc and α-sarcomeric actin (used as a loading control) antibodies.
(*B*) Western blot analysis of transgene expression in different tissue types, performed with total protein extracts from the indicated tissues using myc and α-sarcomeric actin (control) antibodies.
TA = Tibialis Anterior; Gastroc = Gastrocnemius; Soleus; Heart

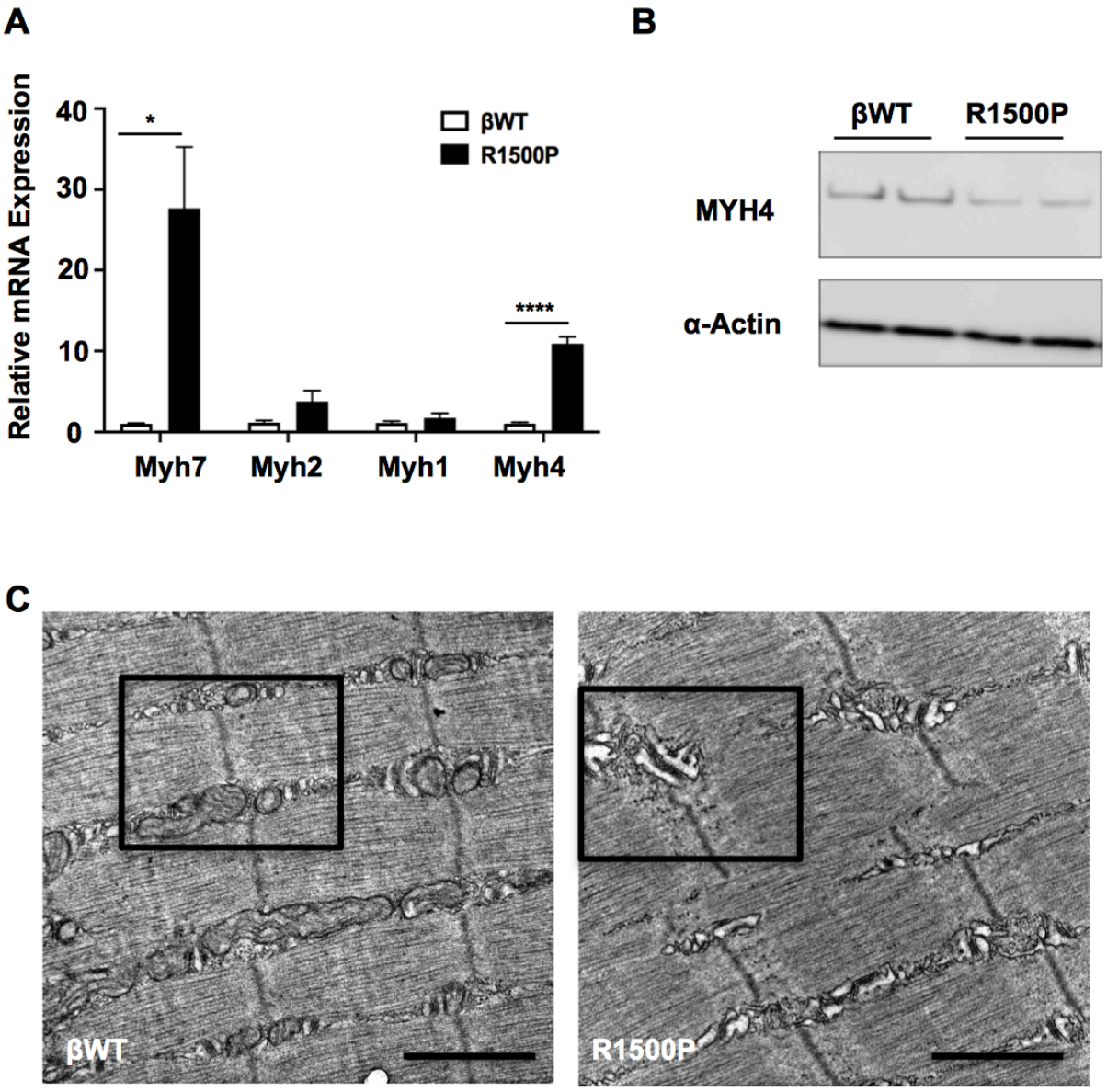

Supplemental Figure 3.2. Characterization of transgenic muscles expressing the mutant R1500P.

(*A*) Relative mRNA expression levels of myosin heavy chain isoforms in the tibialis anterior muscle from 6-to-8-month old βWT and R1500P mice (n = 10/group).

(*B*) Representative Western blot analysis of total protein extracts purified from tibialis anterior (TA) and probed with MYH4 and α-sarcomeric actin (used as a loading control) antibodies.

(*C*) Electron microphotographs of longitudinal sections of TA muscles isolated from 8-month-old WT and R1500P mice. White boxes represent images featured in Figure 2. Bar(s) corresponds to 400 nm.

Data are expressed as mean +/- SEM. *p < 0.05, ****p < 0.0001 by two-tailed unpaired t-test with Welch's correction.

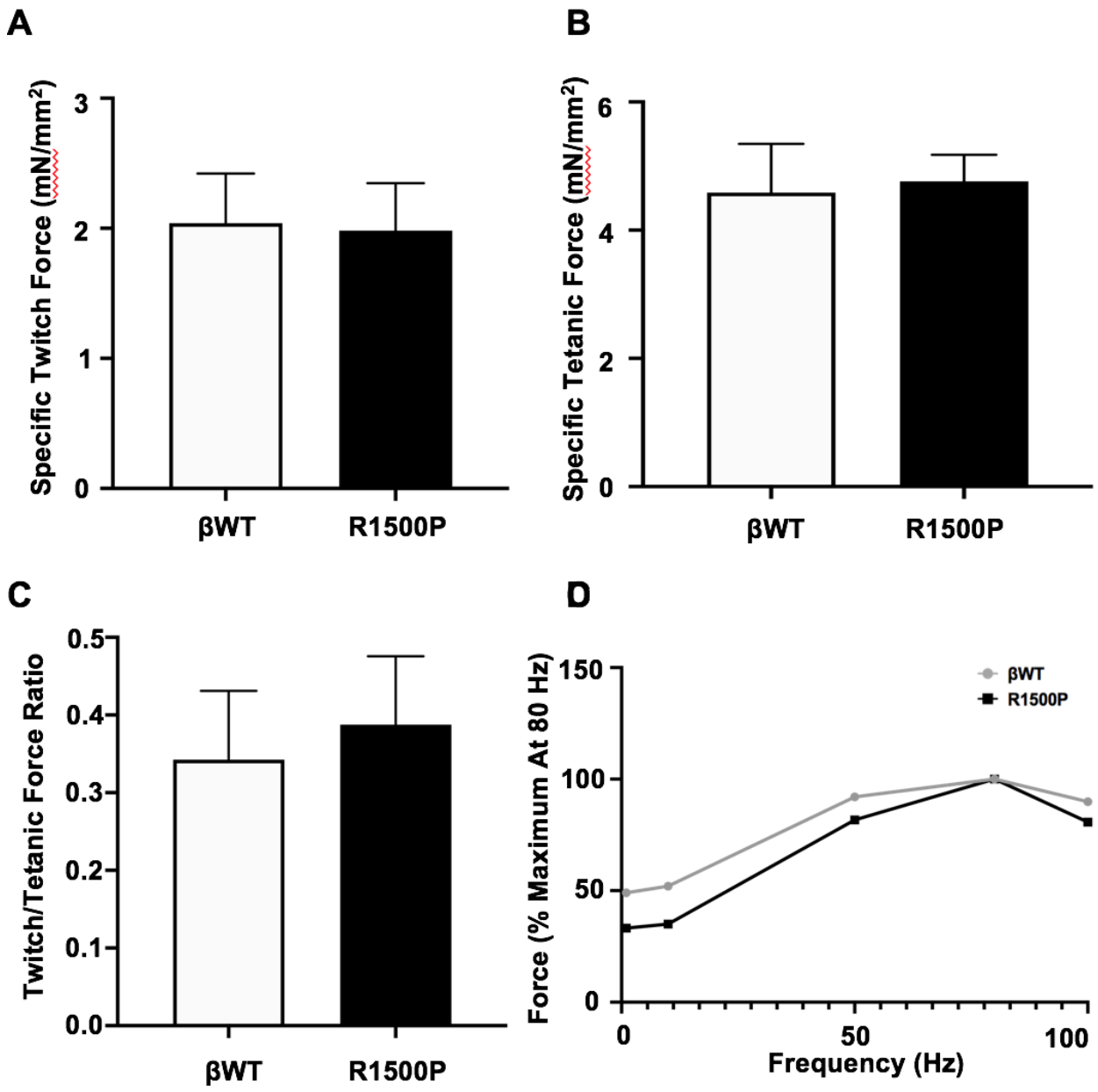

Supplemental Figure 3.3. No change in contractility of intact soleus muscle from transgenic mice.
Soleus muscles isolated from 8-month-old βWT and R1500P mice were subjected to *ex-vivo* contractility assay. Measurement and comparison of basal specific twitch force (*A*), specific tetanic force (*B*), their ratio (*C*), as well as force vs frequency (*D*) are reported. Stimulatory trains of varying frequency (1-100 Hz) were used to generate force-frequency curves. Tetanic force was achieved using 100 Hz.
(*A)* through (*C)*: βWT, n = 5/group; R1500P, n = 3/group. (*D)*: βWT, R1500P n = 1/group. Data are expressed as mean +/- SEM.

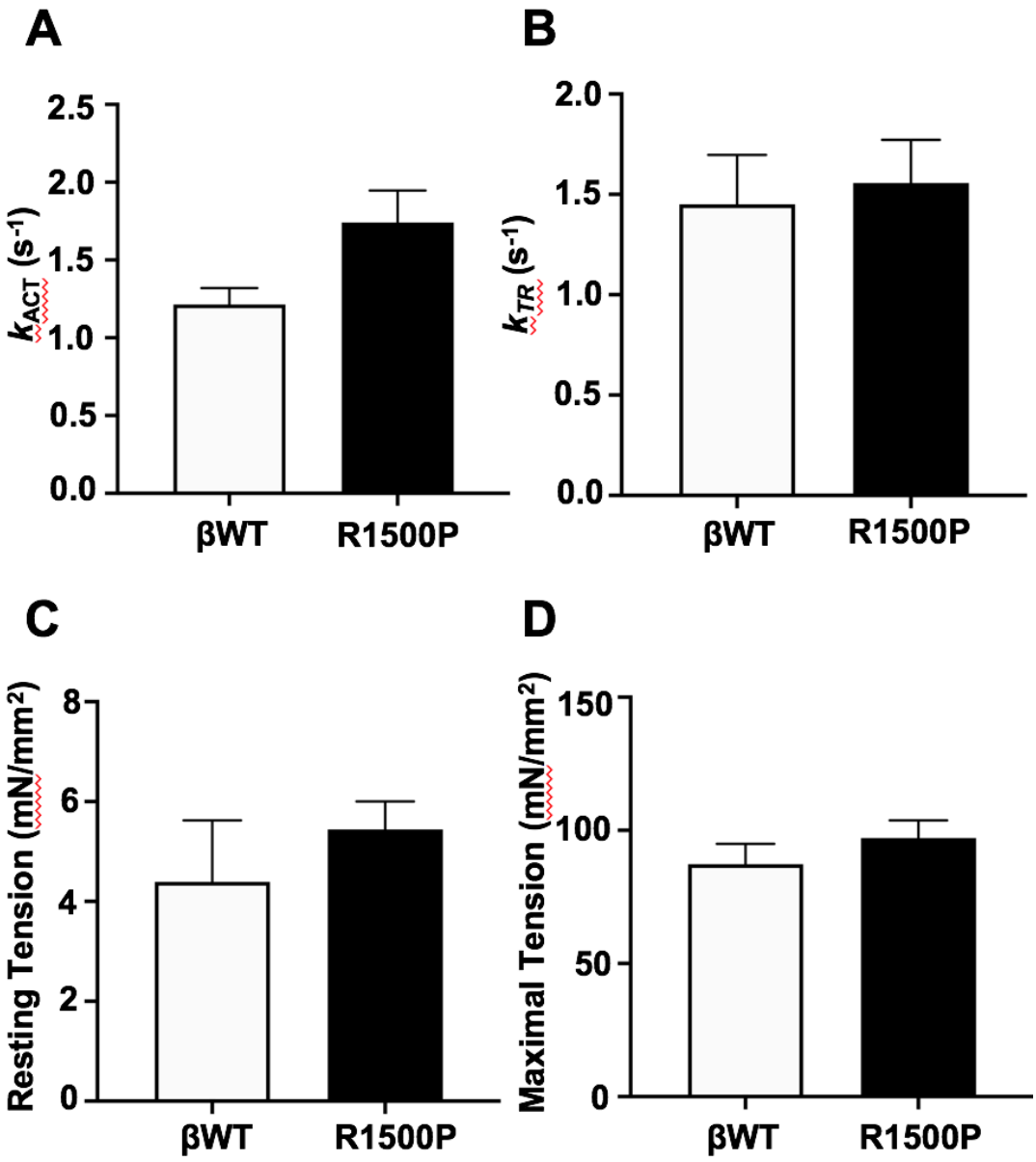

Supplemental Figure 3.4. R1500P mutation does not affect mechanical parameters of myofibril contractility.
Rate constant of tension development (k_{ACT})(*A*), rate constant of tension redevelopment following release-restretch (k_{TR})(*B*) and resting/maximal tension (*C, D*) measured from βWT and R1500P myofibrils. Myofibrils were isolated from TA muscles of 6-month-old βWT and R1500P mice.
Data are expressed as mean +/- SEM of 6-8 myofibrils/tibialis anterior muscle. βWT, n = 3/group; R1500P, n = 5/group.

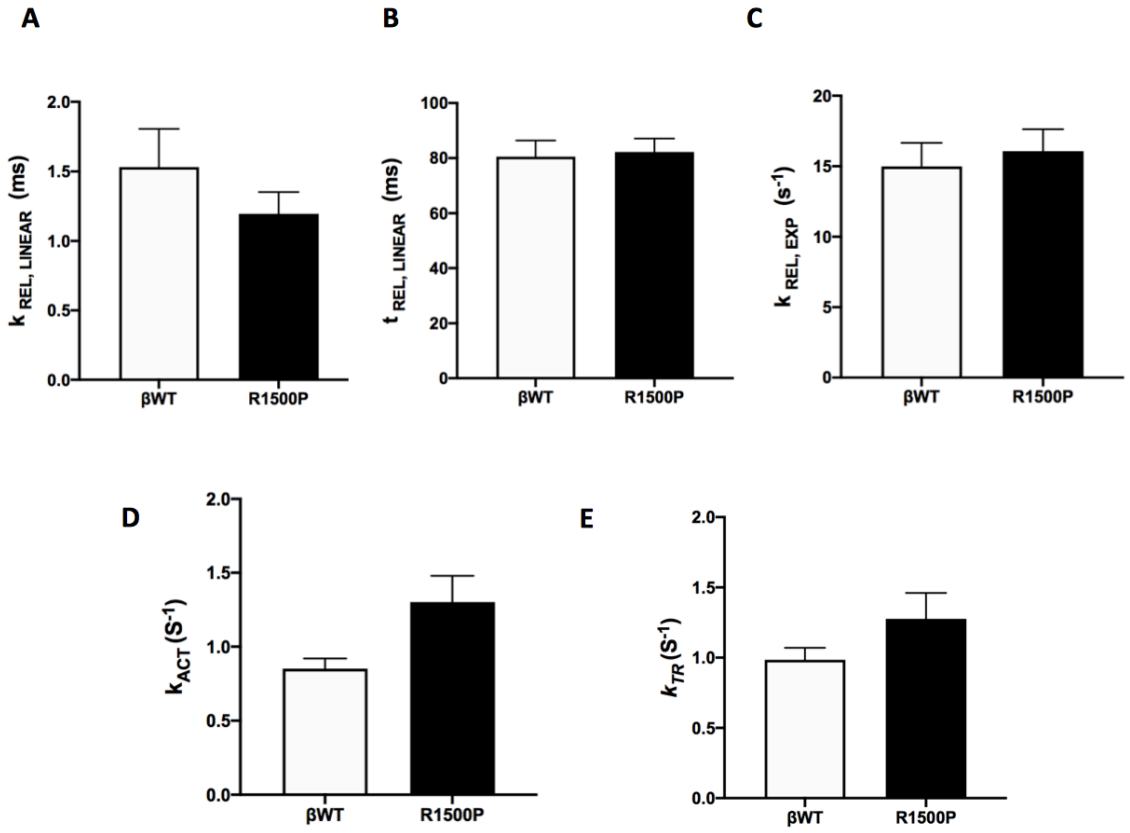

Supplemental Figure 3.5. No difference in activation or relaxation was observed in myofibrils purified from βWT and R1500P soleus muscles.
Rate constant ($k_{REL, LINEAR}$) and duration ($t_{REL, LINEAR}$) of the early linear phase of relaxation (*A*; *B*), rate constant of the final exponential phase of force decline ($k_{REL, EXP}$)(*C*), rate constant of tension development (k_{ACT})(*D*) and rate constant of tension redevelopment following release-restretch (k_{TR})(*E*) measured from βWT and R1500P myofibrils. Myofibrils were isolated from soleus muscles of 6-month-old βWT and R1500P mice.
Data are expressed as mean +/- SEM of 6-8 myofibrils/soleus muscle. βWT, n = 3/group; R1500P, n = 5/group.

CHAPTER IV

Conclusions & Future Directions

Summary

The data presented in this thesis explore:

1.) A physiological response to a change in myosin content in fast-type skeletal muscle and what happens when you shift the balance from fast-to-slow.

2.) A pathological response to a mutation in a slow muscle myosin and how a missense mutation leads to a progressive skeletal muscle disease, Laing distal myopathy.

In Chapter II, we generated a mouse model in which we forced expression of β-MyHC, a slow myosin motor, in fast-type skeletal muscle in order to identify a role for β-MyHC in fiber type specification and plasticity. We showed that expression of β-MyHC was able to drive a fast-to-slow fiber type shift coupled to changes in mitochondrial function suggesting a greater role for β-MyHC expression in fiber type specification than previously thought. In Chapter III, we created the first MPD1 mouse model expressing the R1500P rod mutation. Since the observed phenotypes of the transgenic mice closely mimic MDP1, we believe that our animal model will be a useful platform for testing and developing future therapeutic interventions for MPD1. Together, this research has further elucidated how changes in myosin isoform expression , specifically β-myosin, are able to drive physiological and pathological responses in skeletal muscle in ways that were previously unidentified. These novel mouse models can be used in future studies

to continue bridging research gaps and to further elucidate new roles for β-MyHC and its effect/role in skeletal muscle.

Current Studies/Future Directions

RNA-Seq Study: Comparing differential gene expression between WT TA, WT soleus and β-MyHC TA

As mentioned in Chapter II of this thesis, an RNA-Seq study was performed to analyze differential gene expression between WT TA, WT soleus and β-MyHC TA in order to determine, on a larger scale, the changes observed between these three groups and what pathways are most highly affected, particularly by the change in β-MyHC expression. This analysis is underway, and the datasets are being finalized in order to further elaborate on the data presented in Chapter II.

An additional RNA-Seq study is being performed to analyze differential gene expression between WT and β-MyHC embryos in order to study a developmental timepoint. This study will help identify if the observed phenotypes are turned on developmentally before muscle contraction/movement occurs or if the fiber-type switch occurs post-natally. As proposed in the Chapter II Discussion, β-MyHC is most likely indirectly activating the downstream physiologic and metabolic changes but it remains to be seen how this is occurring. Is the sarcomere able to recognize the change in myosin isoform content through mechanical means? The ongoing RNA-Seq study will help to answer these questions and to further elucidate how β-MyHC plays a role in muscle fiber-type specification and plasticity.

Cross β-MyHC and mdx mice to determine if increased β-MyHC expression ameliorates Duchenne muscular dystrophy phenotype

Previous studies have shown that muscle fiber type switching is commonly observed in muscle-related diseases including Duchenne muscular dystrophy; however, it is not always observed. In Duchenne muscular dystrophy (DMD), fast-type, or glycolytic fibers, are more susceptible to dystrophic pathology, as observed in humans and the mdx mouse model of DMD (76). Therefore, researchers have studied promoting the slow-type gene program as a strategy to ameliorate the effects of DMD on muscle pathology and function (36, 83). Furthermore, studies have shown that increased expression of PGC-1α rescues dystrophic skeletal muscle by inducing a fast-to-slow fiber type shift (113). Because of these results, we have recently crossed our β-MyHC TG animals with the Duchenne muscular dystrophy mdx mouse model in order to determine if by increasing levels of β-MyHC in a dystrophic background, the phenotype is ameliorated or whether myosin heavy chain expression does not change the effects caused by lack of dystrophin. This collaboration is currently underway with animals being analyzed for common dystrophic markers such as changes in muscle histology, creatine kinase levels, and muscle strength.

siRNA against myc-tag effectively silences transgene expression

siRNA against the myc-tag was designed in order to determine if effective silencing of the transgene was possible in a cell culture model. Efficiency and specificity of allele silencing was tested by co-transfecting NRVMs (neonatal rat ventricular cardiomyocytes) with and without siRNA and different dosages of expression plasmids encoding mCherry tagged WT α-myosin and GFP tagged WT β-myosin (with the myc-tag). Confocal microscopy was used to quantify the specific decrease of the green

fluorescent signal generated by the GFP construct. Phenotypic analysis of NRVMs that were transfected without siRNA showed organized sarcomere formation. Furthermore, fluorescent signal, as measured by confocal microscopy, was of equal intensity for all constructs suggesting good transection efficiency. Co-transfection with the myc-tag siRNA resulted in decrease of the green fluorescent signal generated by the GFP tagged WT β-myosin construct and silencing of the myc-tag; the WT α-myosin construct was unaffected indicating specificity of the siRNA for the myc-tag alone (Figure 4.1). In future experiments, the developed siRNA could be used *in vivo* to test the effects of silencing the β-MyHC transgene, are the observed phenotypes reversible and does a fast-type fiber switch occur?

Allele-specific siRNA results in silencing of R1500P mutation

siRNA RP10 was designed to target MPD1 mutation R1500P (Figure 4.2). Single nucleotide specific siRNA was developed following the protocol established by Schwarz *et al.* for allele specific silencing (114). Efficiency and specificity of allele silencing was tested by co-transfecting NRVMs (neonatal rat ventricular cardiomyocytes) with and without siRNA and different combinations of expression plasmids encoding mCherry tagged WT α-myosin and either GFP tagged mutant myosin or GFP tagged WT β-myosin. Confocal microscopy was used to quantify the specific decrease of the green fluorescent signal generated by the GFP mutant construct. Phenotypic analysis of NRVMs that were transfected without siRNA showed organized sarcomere formation, even in the presence of the mutation, suggesting that the mutation does not affect incorporation of the thick filament into the sarcomere (Figure 4.3). Fluorescent signal, as measured by confocal microscopy, was of equal intensity for all constructs. However, co-transfection with the RP10 siRNA resulted in decrease of the green fluorescent signal generated by the mutant

construct and silencing of the mutation; the WT β-myosin construct was unaffected indicating specificity of the siRNA for the mutation alone (Figure 4.3). The developed RP10 siRNA could be used *in vivo* and tested in the previously generated R1500P mouse model in order to determine if it is effectively able to silence the mutation. Furthermore, it could be used as a potential therapeutic intervention if the observed MPD1 phenotypes were reversed in the mouse model.

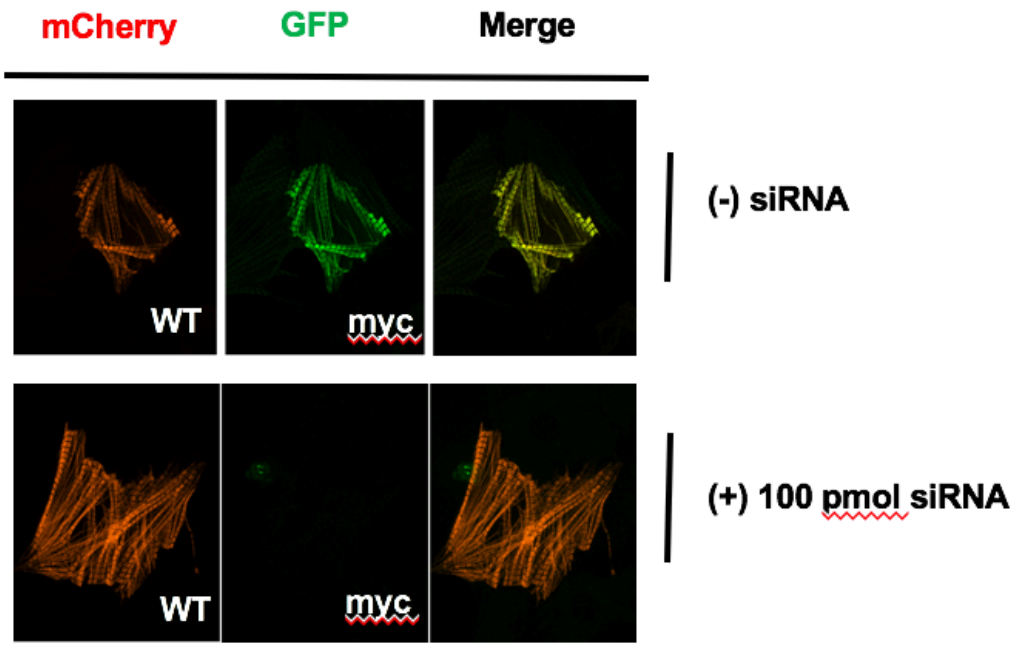

Figure 4.1. myc-tag siRNA effectively silences transgene expression.
Neonatal rat ventricular cardiomyocytes (NRVMs) were transfected with mCherry tagged WTα-myosin and GFP tagged WTβ-myosin (with the myc tag), in the absence and presence of siRNA. Cells were imaged approximately 72 hours after transfection and imaged by confocal microscopy.

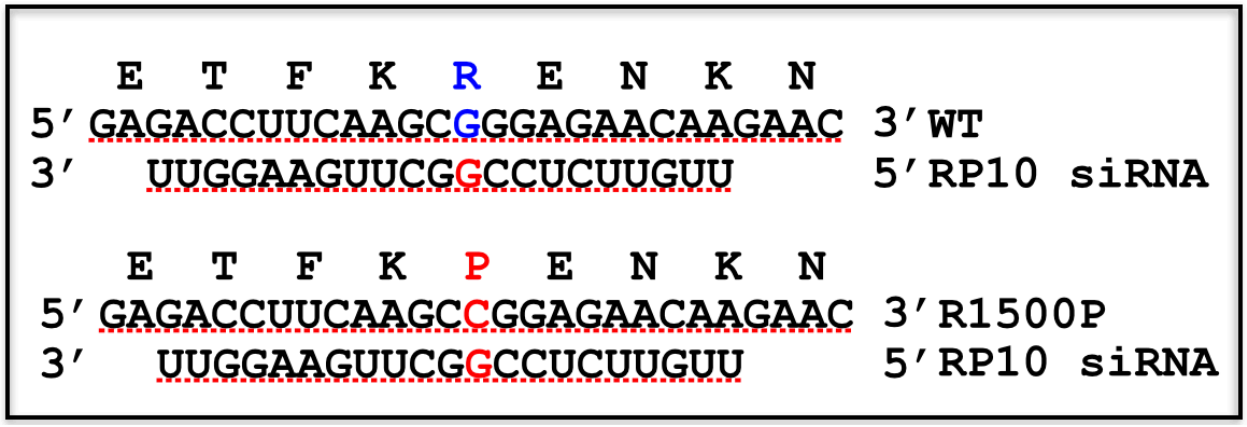

Figure 4.2. RP10 siRNA sequence.
The RP10 siRNA was designed with the mismatched nucleotide located in position 10 of the guide strand. The WT and R1500P sequences are shown.

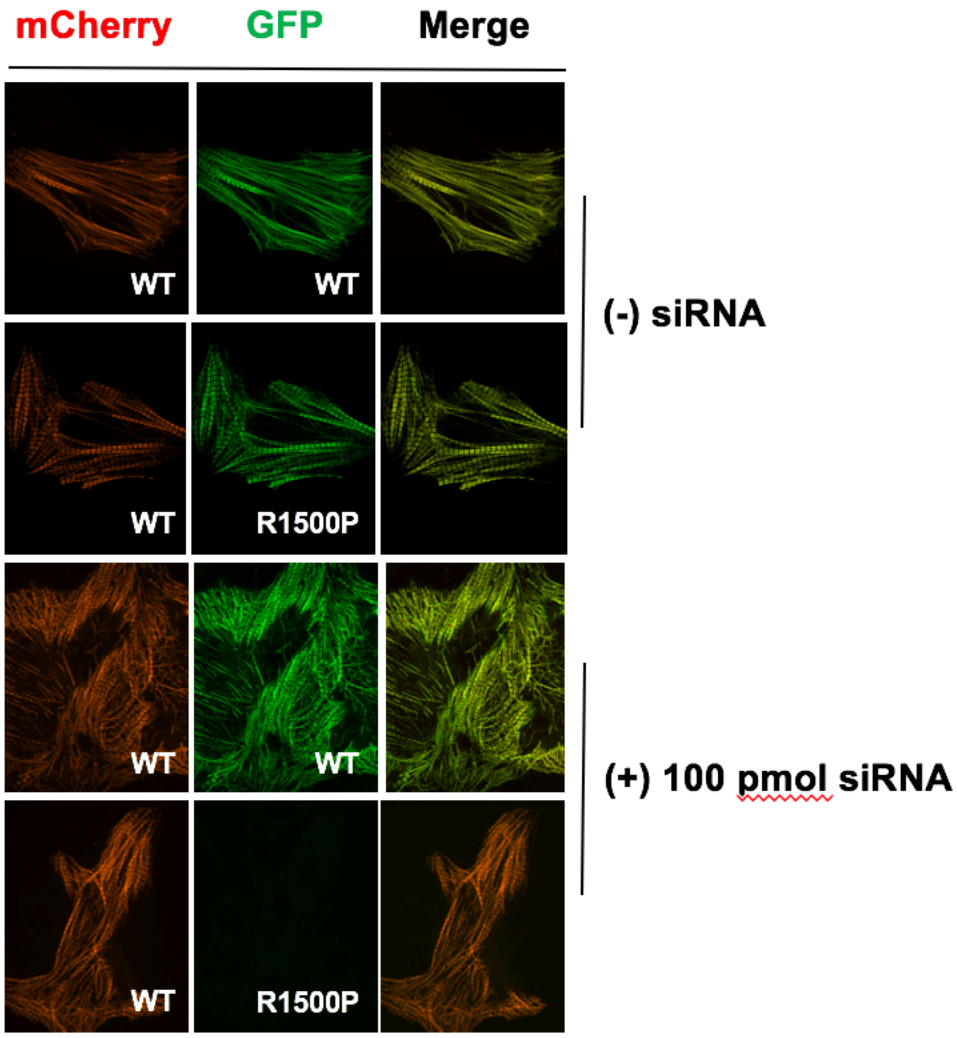

Figure 4.3. Presence of allele-specific siRNA results in silencing of R1500P mutation in NRVMs.
Neonatal rat ventricular cardiomyocytes (NRVMs) were transfected with mCherry tagged WTα-myosin and either GFP tagged WTβ-myosin or R1500P-myosin, in the absence and presence of RP10 siRNA. Cells were imaged approximately 72 hours after transfection and imaged by confocal microscopy.

REFERENCES

1. I. Janssen, S. B. Heymsfield, Z. Wang, R. Ross, Skeletal muscle mass and distribution in 468 men and women aged 18–88 yr. *Journal of Applied Physiology* **89**, 81–88 (2000).

2. A. J. Merrell, G. Kardon, Development of the diaphragm -- a skeletal muscle essential for mammalian respiration. *FEBS J.* **280**, 4026–4035 (2013).

3. R. R. Wolfe, The underappreciated role of muscle in health and disease. *Am J Clin Nutr* **84**, 475–482 (2006).

4. R. Bassel-Duby, E. N. Olson, Signaling Pathways in Skeletal Muscle Remodeling. *Annual Review of Biochemistry* **75**, 19–37 (2006).

5. R. E. Cheney, M. A. Riley, M. S. Mooseker, Phylogenetic analysis of the myosin superfamily. *Cell Motil. Cytoskeleton* **24**, 215–223 (1993).

6. R. Craig, J. L. Woodhead, Structure and function of myosin filaments. *Current Opinion in Structural Biology* **16**, 204–212 (2006).

7. D. A. D. Parry, R. D. B. Fraser, J. M. Squire, Fifty years of coiled-coils and α-helical bundles: A close relationship between sequence and structure. *Journal of Structural Biology* **163**, 258–269 (2008).

8. J. C. Deacon, M. J. Bloemink, H. Rezavandi, M. A. Geeves, L. A. Leinwand, Identification of functional differences between recombinant human α and β cardiac myosin motors. *Cell. Mol. Life Sci.* **69**, 2261–2277 (2012).

9. H. H. Stedman, *et al.*, Myosin gene mutation correlates with anatomical changes in the human lineage. *Nature* **428**, 415–418 (2004).

10. A. Weiss, L. A. Leinwand, The Mammalian Myosin Heavy Chain Gene Family. *Annual Review of Cell and Developmental Biology* **12**, 417–439 (1996).

11. S. Schiaffino, C. Reggiani, Fiber Types in Mammalian Skeletal Muscles. *Physiological Reviews* **91**, 1447–1531 (2011).

12. S. Schiaffino, Fibre types in skeletal muscle: a personal account. *Acta Physiologica* **199**, 451–463 (2010).

13. D. Pette, R. S. Staron, Myosin isoforms, muscle fiber types, and transitions. *Microscopy Research and Technique* **50**, 500–509 (2000).

14. J. Talbot, L. Maves, Skeletal muscle fiber type: using insights from muscle developmental biology to dissect targets for susceptibility and resistance to muscle disease. *Wiley Interdisciplinary Reviews: Developmental Biology* **5**, 518–534 (2016).

15. B. Jostes, C. Walther, P. Gruss, The murine paired box gene, Pax7, is expressed specifically during the development of the nervous and muscular system. *Mechanisms of Development* **33**, 27–37 (1990).

16. M. Goulding, A. Lumsden, A. J. Paquette, Regulation of Pax-3 expression in the dermomyotome and its role in muscle development. *Development* **120**, 957–971 (1994).

17. J. C. Kiefer, S. D. Hauschka, Myf-5 Is Transiently Expressed in Nonmuscle Mesoderm and Exhibits Dynamic Regional Changes within the Presegmented Mesoderm and Somites I–IV. *Developmental Biology* **232**, 77–90 (2001).

18. D. Sassoon, *et al.*, Expression of two myogenic regulatory factors myogenin and MyoD1 during mouse embryogenesis. *Nature* **341**, 303–307 (1989).

19. M. Zhang, I. S. McLennan, During secondary myotube formation, primary myotubes preferentially absorb new nuclei at their ends. *Developmental Dynamics* **204**, 168–177 (1995).

20. J. B. Miller, F. E. Stockdale, Developmental origins of skeletal muscle fibers: clonal analysis of myogenic cell lineages based on expression of fast and slow myosin heavy chains. *PNAS* **83**, 3860–3864 (1986).

21. C. A. Henry, S. L. Amacher, Zebrafish Slow Muscle Cell Migration Induces a Wave of Fast Muscle Morphogenesis. *Developmental Cell* **7**, 917–923 (2004).

22. X. Feng, E. G. Adiarte, S. H. Devoto, Hedgehog acts directly on the zebrafish dermomyotome to promote myogenic differentiation. *Developmental Biology* **300**, 736–746 (2006).

23. A. Draeger, A. G. Weeds, R. B. Fitzsimons, Primary, secondary and tertiary myotubes in developing skeletal muscle: A new approach to the analysis of human myogenesis. *Journal of the Neurological Sciences* **81**, 19–43 (1987).

24. H. E. Jackson, P. W. Ingham, Control of muscle fibre-type diversity during embryonic development: The zebrafish paradigm. *Mechanisms of Development* **130**, 447–457 (2013).

25. J. K.-H. Hu, E. McGlinn, B. D. Harfe, G. Kardon, C. J. Tabin, Autonomous and nonautonomous roles of Hedgehog signaling in regulating limb muscle formation. *Genes Dev* **26**, 2088–2102 (2012).

26. G. Rossi, G. Messina, Comparative myogenesis in teleosts and mammals. *Cell Mol Life Sci* **71**, 3081–3099 (2014).

27. C. Niro, *et al.*, Six1 and Six4 gene expression is necessary to activate the fast-type muscle gene program in the mouse primary myotome. *Developmental Biology* **338**, 168–182 (2010).

28. I. Sakakibara, M. Santolini, A. Ferry, V. Hakim, P. Maire, Six Homeoproteins and a linc-RNA at the Fast MYH Locus Lock Fast Myofiber Terminal Phenotype. *PLOS Genetics* **10**, e1004386 (2014).

29. R. Grifone, *et al.*, Six1 and Eya1 Expression Can Reprogram Adult Muscle from the Slow-Twitch Phenotype into the Fast-Twitch Phenotype. *Molecular and Cellular Biology* **24**, 6253–6267 (2004).

30. S. J. Tapscott, The circuitry of a master switch: Myod and the regulation of skeletal muscle gene transcription. *Development* **132**, 2685–2695 (2005).

31. C. A. Berkes, S. J. Tapscott, MyoD and the transcriptional control of myogenesis. *Seminars in Cell & Developmental Biology* **16**, 585–595 (2005).

32. Y. Liu, A. Chu, I. Chakroun, U. Islam, A. Blais, Cooperation between myogenic regulatory factors and SIX family transcription factors is important for myoblast differentiation. *Nucleic Acids Res* **38**, 6857–6871 (2010).

33. Y. Liu, *et al.*, Six1 Regulates MyoD Expression in Adult Muscle Progenitor Cells. *PLoS One* **8** (2013).

34. E. R. Chin, *et al.*, A calcineurin-dependent transcriptional pathway controls skeletal muscle fiber type. *Genes Dev* **12**, 2499–2509 (1998).

35. E. Calabria, *et al.*, NFAT isoforms control activity-dependent muscle fiber type specification. *PNAS* **106**, 13335–13340 (2009).

36. V. Ljubicic, M. Burt, B. J. Jasmin, The therapeutic potential of skeletal muscle plasticity in Duchenne muscular dystrophy: phenotypic modifiers as pharmacologic targets. *The FASEB Journal* **28**, 548–568 (2013).

37. M. L. Ehlers, B. Celona, B. L. Black, NFATc1 Controls Skeletal Muscle Fiber Type and Is a Negative Regulator of MyoD Activity. *Cell Reports* **8**, 1639–1648 (2014).

38. S. Jäger, C. Handschin, J. St.-Pierre, B. M. Spiegelman, AMP-activated protein kinase (AMPK) action in skeletal muscle via direct phosphorylation of PGC-1α. *PNAS* **104**, 12017–12022 (2007).

39. K. S. C. Röckl, *et al.*, Skeletal Muscle Adaptation to Exercise Training: AMP-Activated Protein Kinase Mediates Muscle Fiber Type Shift. *Diabetes* **56**, 2062–2069 (2007).

40. C. Handschin, *et al.*, PGC-1α regulates the neuromuscular junction program and ameliorates Duchenne muscular dystrophy. *Genes Dev* **21**, 770–783 (2007).

41. A. J. Buller, J. C. Eccles, R. M. Eccles, Interactions between motoneurones and muscles in respect of the characteristic speeds of their responses. *J Physiol* **150**, 417–439 (1960).

42. J. Karp, Muscle Fiber Types and Training. *Strength and Conditioning Journal* **23** (2001).

43. M. M. Bamman, J. K. Petrella, J. Kim, D. L. Mayhew, J. M. Cross, Cluster analysis tests the importance of myogenic gene expression during myofiber hypertrophy in humans. *Journal of Applied Physiology* **102**, 2232–2239 (2007).

44. J. M. Wilson, *et al.*, The Effects of Endurance, Strength, and Power Training on Muscle Fiber Type Shifting. *The Journal of Strength & Conditioning Research* **26**, 1724 (2012).

45. P. J. Lamont, *et al.*, Novel Mutations Widen the Phenotypic Spectrum of Slow Skeletal/β-Cardiac Myosin (MYH7) Distal Myopathy. *Human Mutation* **35**, 868–879 (2014).

46. S. Ortolano, *et al.*, A novel MYH7 mutation links congenital fiber type disproportion and myosin storage myopathy. *Neuromuscular Disorders* **21**, 254–262 (2011).

47. C. J. Tanner, *et al.*, Muscle fiber type is associated with obesity and weight loss. *American Journal of Physiology-Endocrinology and Metabolism* **282**, E1191–E1196 (2002).

48. R. Nilwik, *et al.*, The decline in skeletal muscle mass with aging is mainly attributed to a reduction in type II muscle fiber size. *Experimental Gerontology* **48**, 492–498 (2013).

49. H. Tajsharghi, *et al.*, Myosin storage myopathy associated with a heterozygous missense mutation in MYH7. *Annals of Neurology* **54**, 494–500 (2003).

50. E. Uro-Coste, *et al.*, Striking phenotypic variability in two familial cases of myosin storage myopathy with a MYH7 Leu1793pro mutation. *Neuromuscular Disorders* **19**, 163–166 (2009).

51. E. Pegoraro, *et al.*, MYH7 gene mutation in myosin storage myopathy and scapulo-peroneal myopathy. *Neuromuscular Disorders* **17**, 321–329 (2007).

52. M. V. Shingde, *et al.*, Myosin storage (hyaline body) myopathy: A case report. *Neuromuscular Disorders* **16**, 882–886 (2006).

53. N. Muelas, *et al.*, MYH7 gene tail mutation causing myopathic profiles beyond Laing distal myopathy. *Neurology* **75**, 732–741 (2010).

54. H. Tajsharghi, A. Oldfors, Myosinopathies: pathology and mechanisms. *Acta Neuropathol* **125**, 3–18 (2013).

55. P. Hedera, E. M. Petty, M. R. Bui, M. Blaivas, J. K. Fink, The Second Kindred With Autosomal Dominant Distal Myopathy Linked to Chromosome 14q: Genetic and Clinical Analysis. *Arch Neurol* **60**, 1321–1325 (2003).

56. B. Udd, 165th ENMC International Workshop: Distal myopathies 6–8th February 2009 Naarden, The Netherlands. *Neuromuscular Disorders* **19**, 429–438 (2009).

57. S. Kärkkäinen, *et al.*, Two novel mutations in the β-myosin heavy chain gene associated with dilated cardiomyopathy. *European Journal of Heart Failure* **6**, 861–868 (2004).

58. P. J. Lamont, *et al.*, Laing early onset distal myopathy: slow myosin defect with variable abnormalities on muscle biopsy. *J Neurol Neurosurg Psychiatry* **77**, 208–215 (2006).

59. M. A. Jandreski, M. J. Sole, C. C. Liew, Two different forms of beta myosin heavy chain are expressed in human striated muscle. *Hum. Genet.* **77**, 127–131 (1987).

60. C. Meredith, *et al.*, Mutations in the Slow Skeletal Muscle Fiber Myosin Heavy Chain Gene (MYH7) Cause Laing Early-Onset Distal Myopathy (MPD1). *The American Journal of Human Genetics* **75**, 703–708 (2004).

61. O. Dubourg, *et al.*, A novel MYH7 mutation occurring independently in French and Norwegian Laing distal myopathy families and de novo in one Finnish patient. *J Neurol* **258**, 1157–1163 (2011).

62. N. Darin, H. Tajsharghi, I. Ostman-Smith, T. Gilljam, A. Oldfors, New skeletal myopathy and cardiomyopathy associated with a missense mutation in MYH7. *Neurology* **68**, 2041–2042 (2007).

63. H. Homayoun, *et al.*, Novel mutation in MYH7 gene associated with distal myopathy and cardiomyopathy. *Neuromuscular Disorders* **21**, 219–222 (2011).

64. D. J. Barlow, J. M. Thornton, Helix geometry in proteins. *Journal of Molecular Biology* **201**, 601–619 (1988).

65. T. Z. Armel, L. A. Leinwand, Mutations at the same amino acid in myosin that cause either skeletal or cardiac myopathy have distinct molecular phenotypes. *Journal of Molecular and Cellular Cardiology* **48**, 1007–1013 (2010).

66. F. Parker, *et al.*, A1603P and K1617del, Mutations in β-Cardiac Myosin Heavy Chain that Cause Laing Early-Onset Distal Myopathy, Affect Secondary Structure and Filament Formation In Vitro and In Vivo. *J Mol Biol* **430**, 1459–1478 (2018).

67. M. Buvoli, A. Buvoli, L. A. Leinwand, Effects of Pathogenic Proline Mutations on Myosin Assembly. *J Mol Biol* **415**, 807–818 (2012).

68. M. Dahl-Halvarsson, *et al.*, Drosophila model of myosin myopathy rescued by overexpression of a TRIM-protein family member. *PNAS* **115**, E6566–E6575 (2018).

69. L. Guth, F. J. Samaha, Qualitative differences between actomyosin ATPase of slow and fast mammalian muscle. *Experimental Neurology* **25**, 138–152 (1969).

70. J. R. Zierath, J. A. Hawley, Skeletal Muscle Fiber Type: Influence on Contractile and Metabolic Properties. *PLoS Biol* **2** (2004).

71. M. A. Johnson, J. Polgar, D. Weightman, D. Appleton, Data on the distribution of fibre types in thirty-six human muscles: An autopsy study. *Journal of the Neurological Sciences* **18**, 111–129 (1973).

72. L. E. Aspnes, *et al.*, Caloric restriction reduces fiber loss and mitochondrial abnormalities in aged rat muscle. *The FASEB Journal* **11**, 573–581 (1997).

73. A. E. Civitarese, *et al.*, Calorie Restriction Increases Muscle Mitochondrial Biogenesis in Healthy Humans. *PLOS Medicine* **4**, e76 (2007).

74. K. M. Baldwin, F. Haddad, Invited Review: Effects of different activity and inactivity paradigms on myosin heavy chain gene expression in striated muscle. *Journal of Applied Physiology* **90**, 345–357 (2001).

75. J. F. Marini, *et al.*, Expression of myosin heavy chain isoforms in Duchenne muscular dystrophy patients and carriers. *Neuromuscul. Disord.* **1**, 397–409 (1991).

76. C. Webster, L. Silberstein, A. P. Hays, H. M. Blau, Fast muscle fibers are preferentially affected in Duchenne muscular dystrophy. *Cell* **52**, 503–513 (1988).

77. D. L. Allen, C. A. Sartorius, L. K. Sycuro, L. A. Leinwand, Different Pathways Regulate Expression of the Skeletal Myosin Heavy Chain Genes. *J. Biol. Chem.* **276**, 43524–43533 (2001).

78. J. C. Tardiff, *et al.*, Expression of the β (slow)-isoform of MHC in the adult mouse heart causes dominant-negative functional effects. *American Journal of Physiology-Heart and Circulatory Physiology* **278**, H412–H419 (2000).

79. P. Dunant, *et al.*, Expression of dystrophin driven by the 1.35-kb MCK promoter ameliorates muscular dystrophy in fast, but not in slow muscles of transgenic mdx mice. *Molecular Therapy* **8**, 80–89 (2003).

80. K. H. Park, *et al.*, Ex Vivo Assessment of Contractility, Fatigability and Alternans in Isolated Skeletal Muscles. *J Vis Exp* (2012) https:/doi.org/10.3791/4198 (August 27, 2019).

81. N. L. Reyes, *et al.*, Fnip1 regulates skeletal muscle fiber type specification, fatigue resistance, and susceptibility to muscular dystrophy. *PNAS* **112**, 424–429 (2015).

82. C. Tesi, N. Piroddi, F. Colomo, C. Poggesi, Relaxation Kinetics Following Sudden Ca2+ Reduction in Single Myofibrils from Skeletal Muscle. *Biophysical Journal* **83**, 2142–2151 (2002).

83. A. Chalkiadaki, M. Igarashi, A. S. Nasamu, J. Knezevic, L. Guarente, Muscle-Specific SIRT1 Gain-of-Function Increases Slow-Twitch Fibers and Ameliorates Pathophysiology in a Mouse Model of Duchenne Muscular Dystrophy. *PLOS Genetics* **10**, e1004490 (2014).

84. N. Frey, J. A. Richardson, E. N. Olson, Calsarcins, a novel family of sarcomeric calcineurin-binding proteins. *PNAS* **97**, 14632–14637 (2000).

85. M. Y. Jeong, *et al.*, Histone deacetylase activity governs diastolic dysfunction through a nongenomic mechanism. *Sci Transl Med* **10** (2018).

86. K. C. Woulfe, *et al.*, A Novel Method of Isolating Myofibrils From Primary Cardiomyocyte Culture Suitable for Myofibril Mechanical Study. *Front. Cardiovasc. Med.* **6** (2019).

87. F. Colomo, S. Nencini, N. Piroddi, C. Poggesi, C. Tesi, Calcium dependence of the apparent rate of force generation in single striated muscle myofibrils activated by rapid solution changes. *Adv. Exp. Med. Biol.* **453**, 373–381; discussion 381-382 (1998).

88. C. Tesi, F. Colomo, S. Nencini, N. Piroddi, C. Poggesi, The Effect of Inorganic Phosphate on Force Generation in Single Myofibrils from Rabbit Skeletal Muscle. *Biophysical Journal* **78**, 3081–3092 (2000).

89. C. Tesi, F. Colomo, S. Nencini, N. Piroddi, C. Poggesi, Modulation by substrate concentration of maximal shortening velocity and isometric force in single myofibrils from frog and rabbit fast skeletal muscle. *J Physiol* **516**, 847–853 (1999).

90. B. Brenner, Effect of Ca2+ on cross-bridge turnover kinetics in skinned single rabbit psoas fibers: implications for regulation of muscle contraction. *Proc Natl Acad Sci U S A* **85**, 3265–3269 (1988).

91. A. H. Maass, M. Buvoli, "Cardiomyocyte Preparation, Culture, and Gene Transfer" in *Cardiac Gene Expression: Methods and Protocols*, Methods in Molecular Biology., J. Zhang, G. Rokosh, Eds. (Humana Press, 2007), pp. 321–330.

92. N. G. Laing, *et al.*, Autosomal dominant distal myopathy: linkage to chromosome 14. *Am J Hum Genet* **56**, 422–427 (1995).

93. F. L. Mastaglia, *et al.*, Early onset chromosome 14-linked distal myopathy (Laing). *Neuromuscular Disorders* **12**, 350–357 (2002).

94. M. Dahl-Halvarsson, M. Pokrzywa, M. Rauthan, M. Pilon, H. Tajsharghi, Myosin Storage Myopathy in C. elegans and Human Cultured Muscle Cells. *PLoS One* **12** (2017).

95. L. Murgiano, I. Tammen, B. Harlizius, C. Drögemüller, A de novo germline mutation in MYH7 causes a progressive dominant myopathy in pigs. *BMC Genet* **13**, 99 (2012).

96. A. Maass, L. Leinwand, Animal models of hypertrophic cardiomyopathy. *Current Opinion in Cardiology* **15**, 189–196 (2000).

97. S. Rayavarapu, W. Coley, K. Nagaraju, Endoplasmic Reticulum Stress in Skeletal Muscle Homeostasis and Disease. *Curr Rheumatol Rep* **14**, 238–243 (2012).

98. J. Wu, R. J. Kaufman, From acute ER stress to physiological roles of the Unfolded Protein Response. *Cell Death Differ* **13**, 374–384 (2006).

99. B. Mollereau, S. Manié, F. Napoletano, Getting the better of ER stress. *J Cell Commun Signal* **8**, 311–321 (2014).

100. H.-O. Rashid, R. K. Yadav, H.-R. Kim, H.-J. Chae, ER stress: Autophagy induction, inhibition and selection. *Autophagy* **11**, 1956–1977 (2015).

101. J. J. Hulmi, *et al.*, Effects of muscular dystrophy, exercise and blocking activin receptor IIB ligands on the unfolded protein response and oxidative stress. *Free Radic. Biol. Med.* **99**, 308–322 (2016).

102. C. Moorwood, E. R. Barton, Caspase-12 ablation preserves muscle function in the mdx mouse. *Hum. Mol. Genet.* **23**, 5325–5341 (2014).

103. M. Pauly, *et al.*, ER stress disturbs SR/ER-mitochondria Ca2+ transfer: Implications in Duchenne muscular dystrophy. *Biochim Biophys Acta Mol Basis Dis* **1863**, 2229–2239 (2017).

104. K. Ikezoe, *et al.*, Endoplasmic reticulum stress in myotonic dystrophy type 1 muscle. *Acta Neuropathol.* **114**, 527–535 (2007).

105. R. H. Edwards, D. K. Hill, D. A. Jones, P. A. Merton, Fatigue of long duration in human skeletal muscle after exercise. *J Physiol* **272**, 769–778 (1977).

106. R. E. Hershberger, *et al.*, Coding Sequence Mutations Identified in MYH7, TNNT2, SCN5A, CSRP3, LBD3, and TCAP from 313 Patients with Familial or Idiopathic Dilated Cardiomyopathy. *Clin Transl Sci* **1**, 21–26 (2008).

107. C. F. Kline, P. J. Mohler, "Chapter Four - Evolving Form to Fit Function: Cardiomyocyte Intercalated Disc and Transverse-Tubule Membranes" in *Current Topics in Membranes*, Functional Organization of Vertebrate Plasma Membrane., V. Bennett, Ed. (Academic Press, 2013), pp. 121–158.

108. R. Stehle, J. Solzin, B. Iorga, C. Poggesi, Insights into the kinetics of Ca2+-regulated contraction and relaxation from myofibril studies. *Pflugers Arch - Eur J Physiol* **458**, 337–357 (2009).

109. C. Poggesi, C. Tesi, R. Stehle, Sarcomeric determinants of striated muscle relaxation kinetics. *Pflugers Arch - Eur J Physiol* **449**, 505–517 (2005).

110. P. P. de Tombe, G. J. M. Stienen, Impact of temperature on cross-bridge cycling kinetics in rat myocardium. *J Physiol* **584**, 591–600 (2007).

111. A. Belus, *et al.*, The familial hypertrophic cardiomyopathy-associated myosin mutation R403Q accelerates tension generation and relaxation of human cardiac myofibrils. *J Physiol* **586**, 3639–3644 (2008).

112. P. G. Vikhorev, *et al.*, Author Correction: Abnormal contractility in human heart myofibrils from patients with dilated cardiomyopathy due to mutations in TTN and contractile protein genes. *Sci Rep* **8** (2018).

113. J. T. Selsby, K. J. Morine, K. Pendrak, E. R. Barton, H. L. Sweeney, Rescue of dystrophic skeletal muscle by PGC-1α involves a fast to slow fiber type shift in the mdx mouse. *PLoS ONE* **7**, e30063 (2012).

114. D. S. Schwarz, *et al.*, Designing siRNA That Distinguish between Genes That Differ by a Single Nucleotide. *PLOS Genetics* **2**, e140 (2006).

APPENDIX I: PRIMER SEQUENCES

PRIMER NAME	SEQUENCE
18S_Forward	GCCGCTAGAGGTGAAATTCTTG
18S_Reverse	CTTTCGCTCTGGTCCGTCTT
Myh7_Forward	AGCAGGAGCTGATTGAGACC
Myh7_Reverse	TGTGATAGCCTTCTTGGCCT
Myh4_Forward	ACAGACTAAAGTGAAAGCCTACAA
Myh4_Reverse	CACATTTTGTGATTTCTCCTGTCAC
Myh2_Forward	CCAAGAAAGGTGCCAAGAAG
Myh2_Reverse	CGGGAGTCTTGGTTTCATTG
Myh1_Forward	CGGTGGTGGAAAGAAAGG
Myh1_Reverse	CAGGAGTCTTGGTTTCATT
ATF3_Forward	GCTGCCAAGTGTCGAAACAAG
ATF3_Reverse	CAGTTTTCCAATGGCTTCAGG
GADD34_Forward	GTCCATTTCCTTGCTGTCTG
GADD34_Reverse	AAGGCGTGTCCATGCTCTGG
CHOP_Forward	AGAGTGGTCAGTGCGCAGC
CHOP_Reverse	CTCATTCTCCTGCTCCTTCTCC
ATF4_Forward	GCATGCTCTGTTTCGAATGGA
ATF4_Reverse	CCAACGTGGTCAAGAGCTCAT
PERK_Forward	AGTCCCTGCTCGAATCTTCCT
PERK_Reverse	TCCCAAGGCAGAACAGATATACC
Acta1_Forward	CGACATCAGGAAGGACCTGTATGCC
Acta1_Reverse	AGCCTCGTCGTACTCCTGCTTGG

Ppargc1a_Forward	TCCAGTAGGCAGAGATTTATGAC
Ppargc1a_Reverse	TGTCTGGTTTGACAATCTGCTAGGTC
Ppargc1b_Forward	TCCAGAAGTCAGCGGCCT
Ppargc1b_Reverse	CTGAGCCCGCAGTGTGG
TFAM_Forward	TGGAACACAGCCACATGCTT
TFAM_Reverse	ACCATGGTGGCAAACTGTCT
Tnni1_Forward	TGAAGCCAAATGCCTCCACAACAC
Tnni1_Reverse	ACACCTTGTGCTTAGAGCCCAGTA
Tnni2_Forward	AGCAGCAAGGAGCTGGAAGA
Tnni2_Reverse	ATGGCGTCGGCAGACATAC
Fnip1_Forward	TCCGTCAGTGCCTGGTATC
Fnip1_Reverse	ACAGCTTCTGCTATTGGTTCATC
mt-Nd2_Forward	CCATCAACTCAATCTCACTTCTATG
mt-Nd2_Reverse	GAATCCTGTTAGTGGTGGAAGG
mt-Co1_Forward	ACCATCATTTCTCCTTCTCCTA
mt-Co1_ Reverse	TAGATTTCCGGCTAGAGGTG
mt-Co2_ Forward	TGAAGACGTCCTCCACTCATG
mt-Co2_ Reverse	CCCTGGTCGGTTTGATGTTA
mt-Atp6_ Forward	CATAAATCTAAGTATAGCCATTCCAC
mt-Atp6_ Reverse	AGCTTTTTAGTTTGTGTCGGAAG
mt-Cytb_ Forward	CATTTATTATCGCGGCCCTA
mt-Cytb_ Reverse	TGGGTTGTTTGATCCTGTTTC
Ndufa1_ Forward	TGATGGAACGCGATAGACG
Ndufa1_ Reverse	GCCAGGAAAATGCTTCCTTA

Ndufaf4_ Forward	AAAATGAGAGCTGAGAGAGCTGTT
Ndufaf_ Reverse	CTTTACCCAAACCACCCACT
Sdhd_ Forward	CCTGCTCTGTGGTGGACTACT
Sdhd_ Reverse	CCCATGAACGTAGTCGGTAAC
Cox7a1_ Forward	CGAAGAGGGGAGGTGACTC
Cox7a1_ Reverse	AGCCTGGGAGACCCGTAG
Cox7b_ Forward	AACGCACTAAGCCGTCTCC
Cox7b_ Reverse	CATGGAAACTAGGTGCCCTCT
Atp5e_ Forward	CAAAGCGAACGCTGAGAAG
Atp5e_ Reverse	TCAGCACTTCAGGCTTCAGA
Atp5l_ Forward	AAAACTGGTAGCTTCAAACACCTT
Atp5l_ Reverse	ACAATGCCACGTTTGCCTAT
Ldha_Forward	TGCCTACGAGGTGATCAAGCT
Ldha_Reverse	GCACCCGCCTAAGGTTCTTC
Ldhb_Forward	AGTCTCCCGTGCATCCTCAA
Ldhb_Reverse	AGGGTGTCCGCACTCTTCCT
Lpl_Forward	TTTGTGAAATGCCATGACAAG
Lpl_Reverse	CAGATGCTTTCTTCTCTTGTTTGT